FORMWORK PRESSURE AND RHEOLOGY OF SELF CONSOLIDATING CONCRETE

BY

KAVYA VALLURUPALLI

THESIS

Submitted in partial fulfillment of the requirements
for the degree of Master of Science in Civil Engineering
in the Graduate College of the
University of Illinois at Urbana-Champaign, 2017

Urbana, Illinois

Adviser:

Professor David A Lange

ABSTRACT

The objective of this work was to understand the mechanisms responsible for formwork pressure drop over time in case of self consolidating concrete (SCC). The fresh state properties of SCC, mortar, and cement paste mixes like workability, static yield stress gain and temperature change over time were evaluated and correlated with the formwork pressure data. The mix parameters for the concrete, mortar mixes like water to cementitious ratio, the addition of fly ash, aggregate content, maximum aggregate size, aggregate moisture content, addition viscosity modifying agent, the addition of fibers were investigated. Emphasis was also placed on studying the influence of formwork dimensions on the formwork pressure. The results showed that the formwork pressure drop over time was highly dependent on the thixotropy which can be measured from static yield stress and dynamic yield stress gain over time. So a method for achieving the accurate yield stress values using the ICAR rheometer was developed. The accuracy of the pressure data obtained using the pressure sensors was also evaluated. Based on the results obtained, the accuracy of the Lange and Tejeda model in predicting the formwork pressure of self consolidating concrete was studied. The results showed that within first few hours of the pressure decay, the reversible changes in concrete dominate the pressure decay and slight variation in the mix proportions, mixing procedure alter the pressure decay significantly indicating the sensitivity of SCC mixes. The formwork dimensions also affect the pressure decay indicating the importance of including the formwork dimension parameter while developing the models for prediction of formwork pressure. Recommendations were made for reducing the variation in the mix properties, the importance of focussing on the particle to particle interaction within concrete for understanding its thixotropic properties that seem to be the primary cause of the pressure decay in the initial hours after casting before the hydration process becomes dominant.

Keywords: SCC, formwork dimensions, lateral pressure, rheology, thixotropy, structural buildup, aggregate absorption, static yield stress, dynamic yield stress.

ACKNOWLEDGEMENTS

I would like to thank my advisor Professor David Lange for his valuable guidance throughout the project. I would also like to thank Professor John Popovics and Professor David Lange for letting me be the teaching assistant for CEE 300.

I would like to thank Dr. David Farrow and James Bittner for their help with the pressure sensors, data acquisition systems, and LabVIEW software. I also like to thank Tim Prunkard, Darold Marrow, Jamar Brown, and the undergraduate students Dan, Nanaissa, and Ivan for their help in the experimental preparation. I wish to thank my colleagues from the construction materials group and CEE 300 for their friendship and making the research and teaching work fun.

I want to thank my parents and my brother for their unfailing support and continuous encouragement throughout my years of study and throughout the process of researching and writing this thesis. This accomplishment would not have been possible without them. I also would like to thank my roommates without whom my stay in the USA would have been tough.

TABLE OF CONTENTS

LIST OF TABLES

LIST OF FIGURES

CHAPTER 1

INTRODUCTION

Self consolidating concrete (SCC) is a highly flowable concrete and achieves good consolidation without any need for mechanical vibration. SCC was first developed in Japan in 1988 to improve the durability of the concrete structures [1]. Along with its high flowable nature, SCC also needs to possess excellent segregation resistance (composition should remain uniform throughout the process of transport and placing). As a result, the composition of SCC mix varies from the conventional concrete. SCC mixes usually contains higher powder content, i.e., high amount of portland cement and also uses supplementary cementing materials like fly ash, silica fume or slag. SCC also uses relatively high amounts of chemical admixtures like high range water reducing admixtures to achieve high flowability without increasing the water to cementitious ratio (w/cm) and viscosity modifying admixtures to improve the segregation resistance.

The highly fluid nature of SCC makes it suitable for placing in difficult conditions and sections with congested reinforcement. The absence of mechanical vibration makes the casting process easier and also reduces the noise pollution. Use of SCC also results in the better surface finish, improves production efficiency, and reduces issues with durability.

The high flowability of SCC in its fresh state is due to its low yield strength and plastic viscosity. As a result, when SCC is cast into the formwork, it exerts higher lateral pressure on the formwork as compared to the conventional concrete. As a result, formworks for SCC are usually designed to account for the maximum lateral pressure possible, i.e., the hydrostatic pressure, until the effect on formwork pressure is understood [2]. This approach increases the cost of construction, limits casting rate, and maximum allowable placing height which is supposed be an advantage of using

SCC. The primary objective of this project is to understand the mechanisms responsible for the formwork pressure drop in SCC over time and to improve the methodology for the measurement and modelling of the formwork pressure.

To achieve the objectives mentioned above, various experiments have been conducted. The current study involves preparing various concrete and mortar mixes, studying the formwork pressure decay using PVC columns of different dimensions and understanding how the thixotropic properties of concrete/mortar influence pressure changes (in the formwork) over time. Chapter 2 presents the literature review on the existing knowledge related to formwork pressure in self consolidating concrete (SCC) and methods available for measuring rheological properties of concrete with an emphasis on thixotropy. Chapter 3 presents the description of the materials used and experimental methods in detail. The lateral pressure, temperature, and rheological properties variations over time measured for different SCC, mortar, cement mixes are presented in Chapter 4. The underlying mechanisms for the pressure, temperature, rheology changes are also discussed in Chapter 4. Conclusions and recommendations are presented in Chapter 5, and the references are provided in Chapter 6.

CHAPTER 2

LITERATURE REVIEW

As mentioned in the previous section, the pressure exerted by SCC on the formwork is higher than that of conventional concrete due to its low yield strength and plastic viscosity. As a result, the formworks for SCC are usually designed to sustain the hydrostatic pressure of concrete leading to high cost of formworks.

Experiments conducted by various researchers showed that the maximum pressure exerted by SCC is lower than the hydrostatic pressure. It was also observed that the pressure exerted by SCC on formwork starts to decrease within the first few minutes (referred as pressure decay from here on) of casting. An accurate estimation of formwork pressure is necessary for the design of formwork as under-estimation may result in failure of the form and over-estimation increases the cost of formwork.

So in this chapter, the emphasis is placed on studying the parameters that effect formwork pressure decay and the knowledge needed to understand the mechanism behind the pressure decay.

2.1 Factors affecting pressure decay

Maximum formwork pressure exerted and pressure decay are affected by concrete mix constituents (and their proportions), mixing and placing conditions [3]. The detailed effect of these factors on the formwork pressure are described in the following subsections.

2.1.1 Mix Design Parameters

2.1.1.1 Mineral Admixtures (Fly Ash)

Based on the review of the literature by Gardner [4], use of fly ash as a partial replacement of cement in concrete increases the mobility of concrete and reduces the rate of strength gain. As a result, such concrete exerts a higher pressure on formwork compared to conventional concrete (contains only cement) with similar slump value. He also stated that broadly any mineral admixture that reduces the rate of strength gain of the concrete would increase the lateral pressure on the formwork.

Burak et al. [5] studied the effect of class C fly ash on the viscosity of the paste phase in repair mortars. From the viscosity results, the authors observed that replacement of cement with fly ash increased the viscosity of the mix and as the replacement percentage increased there was no reduction in viscosity even at high shear rates. To understand the underlying mechanisms for this rheological behavior, the micro shape, surface texture, angularity and the particle size distribution of the powders were characterized. From the results obtained, the authors concluded that the high viscosity values for the fly ash incorporated mixes are due to the water and High Range Water Reducing (HRWR) admixture adsorption capacity of fly ash particles, and negative zeta potential of the fly ash powder (-38.7 mV).

Assaad [6] concluded that initial lateral pressure and the rate of pressure drop over time are significantly affected the type of binder and the binder content. For a given binder content, the authors considered mixes with just cement, quaternary (6% silica fume (SF), 28% fly ash (FA), 16% granulated blast furnace slag (BFS), and 72% cement), binary (8% silica fume and 92% cement), and ternary (6% silica fume, 22% fly ash, and 72% cement) powders. It was observed

that the concrete made with just using cement exhibited highest initial pressure and lowest rate of drop in pressure. The authors stated that the addition of SF, FA, and BFS as a partial replacement for cement resulted in increased packing density which could increase the magnitude of flocculation and inter-particle links thereby leading to high degree of particle interlock. Increased interlock makes the concrete less dilatant thereby only a small portion of the weight of concrete need to be supported by the formwork. The thixotropy data presented also supported the argument, i.e., thixotropy for just cement mix was lower compared to mixes made with partial replacement with BFS, SF, and FA.

2.1.1.2 Chemical Admixtures (Viscosity Modifying Admixture)

Viscosity Modifying Admixture (VMA) is added to SCC to enhance the stability of mix. It is often used along with High Range Water Reducing (HRWR) admixture to ensure the flowability with sufficient segregation resistance. Khayat [7] reviewed the types and mode of action of commonly used VMAs and their influence on the rheological properties water and cement paste. The author stated that the mode of action of a VMA (adsorption, association or intertwining) depends on the type and concentration of the polymer used. The authors also observed that the cement paste containing VMA exhibits highly pseudoplastic and thixotropic behavior. Assaad [6] studied the effect of type of VMA and its concentration on the formwork pressure decay and the thixotropic behavior of SCC. Based on the experimental observation, the author concluded that independent of the type of VMA used, the addition of VMA at low concentrations reduces the maximum lateral pressure exerted on formwork, increases the rate of pressure drop, and reduces the elapsed time before pressure cancellation. Based on rheology data, it was concluded that the mixtures with VMA developed a high degree of thixotropy. Ghio et al. [8] studied the effect of VMA

(polysaccharide gums) on the rheology of cement paste. He observed that at low shear rates, the addition of polysaccharide gums to cement paste results in higher viscosity values.

2.1.1.3 Aggregate Properties

Aggregate properties like the maximum aggregate size, particle size distribution, its proportion in concrete, shape, its moisture content, and absorption capacity effects the formwork pressure decay. Rodin [9] concluded that the arching action of the aggregates affects the general shape of the pressure distribution against the formwork. For concrete, as the arching action increases, the lateral pressure deviates more from the equivalent hydrostatic pressure of a fluid having the same density. As per Omran et al. [10] and Amziane et al. [11], the effects of aggregate on formwork pressure can be attributed to several mechanisms. The increase in coarse aggregate content increases the internal friction and shear strength that can contribute to the rate of stiffening of concrete and plastic viscosity. Fine aggregate offers numerous nucleation sites for precipitation of hydration products so increasing the fine aggregate content increases the rate of pressure drop. Aggregate absorption also affects the lateral pressure, as the aggregates absorb water the effective water-to-cementitious materials ratio (*w*/cm) of the mix and the ionic strength in the pore solutions changes. Assaad et al. [11] studied the effect maximum aggregate size (MSA) on the lateral pressure exerted by SCC. The authors used three grades of crushed limestone aggregate with size fractions of 10-5, 14-5, and 20-5 mm. The authors observed the pressure drop is more drastic when 14 mm MSA was used compared to 10 mm MSA. However the different seemed less between 20 mm MSA and 14 mm MSA. The author attributed this behavior to the aggregate packing densities (56% for 10 mm MSA, 62% for 14mm MSA, and 60% for 20 mm MSA).

Omran et al. [10] studied the effect of increasing the coarse aggregate volume from 270 L⁄m^3 to 330 L⁄m^3 and reduction of sand to total aggregate ratios (S/A) from 0.52 to 0.44 on lateral pressure. The authors observed that the increasing the coarse aggregate volume or the reduction in S/A ratio leads to a reduction in lateral pressure. This reduction in lateral pressure is attributable to the fact that the increase in aggregate content (coarse aggregate and sand) reduces the paste volume, and consequently leads to increased internal friction and lower lateral pressure.

Billberg [13] studied the effect of different types of fine aggregate used on the fresh properties (slump loss) of SCC. The author observed that the mixes with the aggregates with relatively higher fineness values have faster slump-loss and he also noted that type of aggregate used also affects the effectiveness of the High Range Water Reducing (HRWR) admixture.

2.1.1.4 Water to Cementitious ratio

Roby [14] made a series of tests using the concrete mixes of different water to cementitious ratios (w/cm), different cement contents to determine the effect of both cement and water contents on the form pressure. He observed two concrete mixes with water to cementitious ratios 0.91 (normal mix - slump 7 in.) and 0.86 (dry mix - slump 3 in.). The results showed that the maximum pressure was 20 to 25 percent less for dry mix compared to the normal mix. The author suggested that as the w/cm increases there is a reduction in the strength of the mortar causing the concrete to be more fluid. The high fluidity of concrete reduces the deviation of lateral pressure of concrete from the hydrostatic pressure distribution.

Bensted [15] studied the effect of w/cm on the early hydration of Portland cement and white cement. He concluded that as the w/c ratio is progressively raised from 0.3 through 0.4 to 0.5, increased quantities of ettringite are formed at all the hydration times studied from five minutes to

two hours. He also noted that C-S-H was not formed in detectable quantities within first two hours of hydration. Khayat et al. [16] concluded that change in w/cm ratio has a significant effect on the formwork pressure and thixotropy. The authors observed three different SCC mixes with w/cm ratios 0.46, 0.40 and 0.36. As per their results, SCC mix with w/cm 0.46 exhibited lower thixotropy and greater initial pressure compared to other two mixes. Based on this observation, the authors concluded that the increased water and paste contents and reduction in coarse aggregate volume lead to lower shear strength properties of the plastic concrete in the mix with 0.46 w/cm. The authors also observed that the rate of drop in formwork pressure and rate of gain in the thixotropy with time are faster in 0.46 w/cm ratio mix compared to other two. The authors considered this is probably due to the greater HRWRA demand in the low w/cm ratio mixes thereby reducing fluidity loss with time and build up in cohesiveness.

2.1.2 Placing Conditions

Placing conditions like the casting rate and casting method seem to affect the formwork pressure characteristics.

2.1.2.1 Casting Rate

Rodin [9] concluded that the rate of pour increases both P_m (maximum concrete pressure) and H_m (head of concrete at maximum pressure). Also as the rate of pouring increases, H_m increase at a decreasing rate, indicating that at low rates of pouring the hardening of the cement has a more important effect than the arching action. Billberg [13] showed that the casting rate correlates to the maximum formwork pressure and the authors concluded that as casting rate decreases the maximum formwork pressure decreases because as the concrete is at rest for longer time (due to slower casting rate), concrete could resist vertical load better without increasing the lateral

pressure. Gardner [4] also had a similar conclusion, and the authors stated that the casting rate increases the time necessary to fill the formwork. As a result, the time available for concrete to develop shear strength decreases thereby resulting in higher lateral pressure. Omran et al. [17] also observed that maximum lateral pressure is higher (approx. by 9 to 10%) in the case of faster casting rate (20m/h) compared casting rate of 5m/h.

2.1.2.2 Casting Methods

The influence of casting method, i.e., pouring the concrete into the formwork from above vs. pumping the concrete into the formwork from below was investigated by Leemann [18]. The authors found that when the concrete is cast from the bottom, the lateral does not decrease below the hydrostatic pressure during casting because the concrete is constantly in motion. The authors also stated that the formwork pressure could locally exceed the hydrostatic pressure while casting due to the influence of the pump because the pump has to overcome the weight of the concrete already in the formwork.

2.1.3 Formwork Characteristics

As per ACI 347-04 [2], the cost of formwork in the US can be as much as 60% of the total cost of the completed concrete structure in place and sometimes greater. Formwork characteristics are highly important in the case of SCC because due to its flowability SCC exerts higher lateral pressure thereby increasing the risk of failure. Selection of formwork also affects the speed, efficiency of the construction process, and quality of the finished surface. As a result, several researchers have performed studies to understand the effect of formwork characteristics on the lateral pressure characteristics of SCC. Shape, size, and the properties of the formwork material

(stiffness, water absorption capacity, volume stability of the material, etc.) affect the formwork pressure characteristics (Omran et al. [17])

2.1.3.1 Formwork Shape

Most commonly circular and rectangular shaped formworks are used for casting of concrete. Most of the researchers used circular formwork for studying SCC [6], [19], [20]. Rectangular formwork was used by Arslan et al. [21]. The effect of formwork shape on the formwork pressure was studied by Omran et al. [17] for SCC and conventional concrete by Santilli et al. [22]. Both the researchers concluded that the formwork shape has little to no influence on the lateral pressure exerted by fresh concrete on formwork.

2.1.3.2 Formwork Size

Effect of formwork size on the formwork pressure is studied by various researchers [2], [6], [9], [17], [23], [24]. CIRIA Report 108 [24] and ACI 347 [2] propose different prediction models for the formwork pressure depending on whether the pressure prediction for wall or column (A wall is defined as having sections where either the width or the breadth exceeds 2 m, while for a column, both magnitudes are less than 2 m). Rodin [9] considered that the smaller the width of the form, smaller would be the maximum lateral pressure due to the increased degree of arching effect. Gardner et al. [23] also demonstrated experimentally that for conventional concrete, an increase in formwork dimension results in an increase in lateral pressure. Gardner [4] also demonstrated theoretically and experimentally that as the minimum dimensions of the member becomes larger the pressure on the formwork increases because the wall shear becomes smaller relative to the mass of the concrete. Santilli et al. [22] also made a similar observation and concluded that

formwork size is an important factor in fresh concrete lateral pressure and its initial rate of pressure decay.

In the case of SCC, Assaad [6] studied the effect of column diameter on the maximum lateral pressure and observed that larger column (column with larger diameter 0.92 m) has slightly higher initial pressure and a higher rate of pressure decay than the column with a lower diameter (0.20 m). Omran et al. [17] Studied the effect of the minimum cross-sectional dimension of formwork on the maximum lateral pressure and the rate of pressure decay using both SCC (two SCC mixes with different thixotropy were studied) and conventional concrete mixes. The authors concluded that the initial maximum lateral pressure increases with the increase in formwork width for a given formwork dimension. The author attributed this behavior to arching effect. The authors also concluded that arching phenomenon could be negligible when using formwork of larger lateral dimensions (approx. above 0.40 m).

2.1.3.3 Properties of Formwork Material

Tejeda [19] studied the effect of formwork material on the formwork pressure characteristics by testing four different formwork systems. All the four formwork systems were designed to have same dimensions. Two formwork systems were made using sonotube (ST) and the other two using PVC. Configuration 1 (ST1) used sonotube as form without any modification (ST1), Configuration 2 (ST2) used sonotube with an impermeable plastic liner applied to cover the internal wall (to prevent the sonotube from getting wet). Configuration 3 (PVC1) used PVC pipe as formwork without any modification and Configuration 4 (PVC2) was also made using PVC pipe but cut along one side from top to bottom, and reinforced with eight steel straps to keep it tightly closed. The results showed that maximum lateral pressure exerted by SCC was not affected however the

rate of pressure decay varied significantly. The author attributed the difference in pressure decay is due to difference stiffness (between PVC1, PVC2, and ST2), the difference in effect moisture from concrete has on the material (Sonotube in ST1 configuration absorbed moisture from concrete thereby modifying the water content of SCC and also swelling of the Sonotube form).

Omran et al. [17] also conducted experiments to study the effect of formwork surface material on the initial pressure and pressure decay. The authors considered four different surface materials (plywood, steel, PVC, and polyester filter). Based on the results obtained the authors concluded that formwork surface material does not have any significant effect on the initial lateral pressure. The authors also suggest that using permeable formwork might result in a change in water content of fresh concrete.

2.2 Existing Mathematical Models

Several models have been developed to predict the maximum lateral pressure exerted by SCC on the formwork. For the development of these models, some researchers have focused on measuring the formwork pressure in the laboratory or field [19], [23]. Others have focused more on different mechanisms such as the material thixotropic properties [25] and the friction between the concrete and the formwork [26], [27], [28]. Some of the models proposed to predict the formwork pressure in SCC or conventional concrete are discussed in detail in the following subsections.

2.2.1 Lange and Tejeda Model [19]

The model is proposed based on the laboratory tests, and the model can be calibrated for the use in the field. The model has been tested in field conditions and seems to predict an accurate maximum concrete pressure value [19], [29]. This model used a PVC column of dimensions 920 mm length and 250 mm in diameter. The PVC column is instrumented with flush mounted pressure

sensors installed at 152 mm from the base. The sensor measures the lateral pressure exerted by concrete on the PVC pipe from the end of casting to the point where pressure drops to zero. The authors attributed the change in pressure (decay in pressure) over time to an increase in the internal friction angle and cohesion over time. The pressure decay with time was fit through a hyperbolic function to give a good fit and also to allow for different patterns with changes in simple parameters and to comply with boundary conditions. The maximum lateral pressure exerted by SCC (P_h) can be predicted as follows:

$$P_h = \gamma R t \frac{C_0}{(at^2 + 1)^{\alpha}} \quad (1)$$

Where

γ is the unit weight of concrete

R is the casting rate

t is time

C_0 is the initial pressure

a and α are variables to fit the function to the pressure decay

2.2.2 CIRIA Model [24]

CIRIA (Construction Industry Research and Information Association) model as reported by Khayat et al. [3] and Gardner [4] is for estimating the formwork pressure in conventional concrete. It considers that the formwork pressure is affected by the rate of placement, formwork characteristics (shape and size), the density of concrete, concrete constituent materials, vibration

time. This method considers that the maximum lateral pressure (P_{max}) exerted by concrete is hydrostatic up to a certain height (h) and this height depends on the arching and stiffening of concrete. Among the equations shown below, Equation (2) is for arching criterion, Equation (3) is for concrete stiffening or hardening criterion, and Equation (4) is the general formula.

$$P_{max} = 14.37 + 0.094d + 3.14R < 24H \; or \; 143.7 \tag{2}$$

$$P_{max} = \frac{\gamma_c RT}{1 + c(\frac{t}{t_{max}})^4} + (4.6 - 1.89R) < 24H \; or \; 143.7 \tag{3}$$

$$P_{max} = \gamma_c \left[C_1\sqrt{R} + C_2 K \sqrt{H - C_1\sqrt{R}} \right] \nsucceq \gamma_c h \tag{4}$$

Where

P_{max} is the maximum lateral pressure (kPa)

γ_c is the unit weight of concrete (kg/m^3)

R is the casting rate (m/h)

d is the minimum formwork dimension (mm)

T is the fresh concrete temperature (ºC)

t is the time after the start of placing (h)

t_{max} is the stiffening or hardening time (h)*

c is the vibrating time*

H is the vertical formwork height (m)

h is the height of fresh concrete above the point considered (m)

C_1 is the cross section coefficient (1.0 for walls & 1.5 for columns)

C_2 is the additive coefficient (0.3 - 0.6)

K is the temperature coefficient = $\left(\frac{36}{T+16}\right)^2$

* c and t_{max} were defined in empirically derived charts.

2.2.3 Gardner's model [4]

For conventional concrete, Gardner [4] observed that the maximum lateral pressure (P_{max}) exerted by concrete depend on the depth of vibration, the rate of pour, concrete temperature, formwork dimension, material constituents and concrete slump. The author considered that the pressure distribution is hydrostatic up to a certain depth and becomes constant thereafter until the bottom of formwork Khayat et al. [3]. The prediction equation is as follows:

$$P_{max} = 24h_i + \frac{3000HP}{d} + \frac{d}{40} + \frac{400\sqrt{R}}{18+T}\left(\frac{100}{100-\%F}\right) + \frac{S-75}{10} < 24H \quad (5)$$

Where

P_{max} is the maximum lateral pressure (kPa)

H is the total height of formwork (m)

h_i is the immersed depth of vibrator (m)

d is the minimum formwork dimension (mm)

HP is the horsepower of vibrator

R is the casting rate (m/h)

T is the concrete temperature (^{o}C)

F is the percentage replacement of cement by fly ash or slag (%)

S is the slump after the application of superplasticizer (mm)

2.2.4 Gardner's New Model [23]

Gardner's new model is for the prediction of maximum lateral pressure for SCC, and it is based on the results obtained from field observations. The authors observed that type and dosage of chemical admixture used (superplasticizer and retarder specifically) not only affected the slump flow and also affected the formwork pressure significantly. The authors suggested that 'any lateral pressure equation for SCC needs to include the rate of concrete placement, a measure of the time for the concrete to achieve strength /stiffness and asymptotic to hydrostatic as placed.' The time (t_0) needed for the slump flow of concrete to reach to zero was chosen as the parameter for characterizing the stiffening/strength behavior of concrete. Since t_0 cannot be measured physically, the parameter is obtained by extrapolating the slump loss from the time for the slump flow to drop to 400 mm from the initial value (t_{400}).

$$t_0 = t_{400}\left[\frac{Initial\ slump\ flow\ (mm)}{(Initial\ slump\ flow\ (mm) - 400)}\right] \quad (6)$$

$$P = wR\left(t - \frac{t^2}{2t_0}\right)\ for\ t < t_0 \quad (7)$$

$$P_{max} = \frac{wRt_0}{2}\ for\ t > t_0 \quad (8)$$

If the time to fill the form, t_h (height of form /rate of placement), is less than t_0 then t_h can be used as t in Equation (7).

$$P_h = wR\left(t_h - \frac{{t_h}^2}{2t_0}\right) \tag{9}$$

Where

h is the height of placement (m)

P_h is the limiting lateral pressure (kPa)

R is the casting rate (m/h)

t_{400} is the time for slump flow to drop to 400 mm (h)

t_h = h/R hours

w is the unit weight of concrete (kg/m^3)

2.2.5 Vanhove's Model [28]

Vanhove's approach for the prediction of the lateral pressure is based on the granular models used for estimating the material's lateral pressure. These granular models predict the lateral pressure based on the knowledge of the friction between the ensiled material and the containing structure. This current model (Vanhove's model) is based on the Janssen's model [30] (as reported by Ovarlez et al. [26]) in which the friction is treated as a Coulomb effect. The Janssen model relates the horizontal pressure (P_h) to the vertical pressure (P_v) with the Janssen parameter (K). The value of K depends on the internal friction angle of the material. Janssen's model also assumes that at all points pressure is at the slip threshold, which is taken in its Coulomb form. So the friction stress

(τ) can be expressed in terms of horizontal pressure (P_h) and friction coefficient (μ). The lateral pressure exerted on the wall is obtained by equilibrating the horizontal forces (exerted by the walls) and the vertical forces acting on the material at rest.

$$P_h(h) = KP_v(h) \tag{10}$$

$$\tau(h) = \mu P_h(h) \tag{11}$$

$$P_h(h) = P_{Janssen}(h) = \frac{\rho g A}{(2e + 2L)\mu K}\left(1 - e^{-\frac{(2e+2L)\mu K}{A}h}\right) \tag{12}$$

Where

$P_h(h)$ is the lateral pressure at depth h

P_v is the vertical pressure

K is the Janssen's Parameter

τ is the friction stress (or tangential stress)

μ is the coefficient of friction

$P_{Janssen}$ is the lateral pressure estimated using Janssen model

ρ is the density of the concrete

e is the thickness of the formwork

L is the width of the formwork

A is the area (e x L)

The authors checked the applicability of the Janssen's model for SCC by casting the formworks, and the friction coefficient between SCC and the formwork was measured using tribometer. Based on the results obtained the author suggested that Janssen model (Equation (12)) underestimates the lateral pressure exerted by concrete and the authors explained that unlike the granular materials, concrete has a shear threshold (yield stress) and so the yield stress should be added to the friction stress (τ in Equation (11)). However, for SCC, the authors state that the shear threshold value can be neglected and the underestimation of the lateral pressure can be rectified by introducing a correction factor (α). The value of the correction factor (α) seems to represent the state of grain–grain and concrete–wall contacts which depend on the casting technique, the rheological characteristics of the concrete, the release agent, etc. The modified equation for the estimation of lateral pressure for SCC is shown below.

$$P_h(h) = \frac{\rho g A - \alpha \tau_0 (2e + 2L)}{\alpha (2e + 2L) \mu K} \left(1 - e^{-\frac{\alpha (2e+2L) \mu K}{A} h}\right) \quad (13)$$

2.2.6 Ovarlez and Roussel's Model [26]

Overlez and Roussel's model follows a theoretical approach, and it considers SCC as an elastic material confined in the formwork and follows Tresca plasticity criterion (i.e., the maximum stress sustainable by an internal plane is the yield stress of the concrete). Janssen model [Section 0] which is used to predict the relation between the horizontal and vertical stress for granular materials in silo cells is used by the authors for predicting the lateral pressure exerted by SCC on formwork (similar to Vanhove's model [Section 0] described above). The authors state that the pressure exerted by concrete at a certain depth (H) is equal to a hydrostatic pressure reduced by the vertical stress at the walls which is between 0 and the concrete yield stress (τ_0). The authors assumed that

the weight of the concrete could cause SCC to deform vertically and this deformation is sufficient to increase the shear stress to the yield stress of concrete (τ_0). The authors observed that the yield stress of concrete increased linearly with time and introduced a time-dependent yield stress parameter (A_{thix}). Based on the assumptions mentioned above and observations the equations needed for the prediction of maximum lateral pressure are proposed.

$$\tau_0(t) = {\tau_0}^i + A_{thix}t \tag{14}$$

$$P_{max} = K\left(\rho g H - \frac{(H-r)^2 A_{thix}}{rR}\right) \tag{15}$$

Where

τ_0^i is the initial yield stress of the SCC

t is resting time (sec)

A_{thix} is the time-dependent yield strength (Pa/s)

P_{max} is the maximum lateral pressure (kPa)

K is the Janssen's parameter

ρ is the density of the concrete (kg/m^3)

H is the total height of formwork (m)

r is the radius of the circular formwork or width of the rectangular formwork (m)

R is the casting rate (m/h).

2.2.7 Graubner and Proske's model [25], [27], [29]

Similar to Overlez and Roussel [Section 0], Graubner and Proske's model also uses Janssen model to predict the relation between the horizontal and vertical stress by SCC on formwork. The authors also assume that the lateral pressure exerted by SCC on formwork depends on the wall friction and the time-dependent behavior of concrete at rest. The time-dependent behavior of concrete at rest was attributed to setting time of concrete. The time-dependent values of friction μ(t) between concrete and the formwork, Janssen's parameter (λ(t)) were determined in laboratory tests. The equations for the prediction of lateral pressure are shown below.

$$P_V = e^{-\int \lambda(t)\mu(t)\nu\frac{U}{A}dt}\left(\int \gamma_c \nu e^{\int \lambda(t)\mu(t)\nu\frac{U}{A}dt}\, dt\right) \quad (16)$$

$$P_h = P_V\, \lambda(t) \quad (17)$$

Where

P_v is the vertical pressure

λ is the Janssen's Parameter

μ is the coefficient of friction

ν is the casting rate

U is the perimeter of the formwork cross-section

A is the area of the formwork cross-section

t is the age of concrete

P_h is the lateral pressure

2.2.8 Khayat and Omran's Model [3], [29]

Empirical models for estimating maximum lateral pressure (P_{max}) were developed. The models were developed by taking one parameter at a time. Then, different combinations between two parameters at a time were investigated. The empirical models for two parameters were derived using linear regression analysis. These derivations were extended to include most significant parameters that affect formwork pressure casting height (H), casting rate (R), minimum lateral dimension of the formwork (D_{min}), structural buildup at rest of the concrete taken as the static yield stress buildup after 15 minutes of rest ($PV\tau_{0rest@15min}$), maximum aggregate size (f_{MSA}) and waiting period between the successive lifts (f_{WP}). The prediction models were based on a large number of laboratory tests conducted using 0.7 m long column with over pressure to simulate the condition of a 13 m long column. Static yield stress buildup was measured using portable vane (PV) empirical test method. The torque required break the structure by the vane and the vane geometry were used to compute the static yield stress value. The rheology tests were conducted at the same temperature as the casting temperature of concrete (T_i).

The validity of the prediction model was tested using field measurement results. The results from field measurements yielded a good correlation with empirically predicted values. The equation for the prediction of lateral pressure is shown below.

$$P_{max} = \frac{\gamma_c H}{100}\left[98 - 3.82H + 0.63R + 11D_{min} - 0.021PV\tau_{0rest@15min@T_i}\right] x f_{MSA} x f_{WP} \quad (18)$$

Where

P_{max} is the maximum lateral pressure

γ_c is the unit weight of concrete (kN/m^3)

H is the casting depth (m)

R is the casting rate (m/h)

D_{min} is the minimum lateral dimension of the formwork (m)

$PV\tau_{0rest@15min}$ is the static yield stress measured at 15 min of rest (Pa)

T_i is the cast temperature of concrete (^0C)

2.3 Rheology

Most of the literature presented in this section is taken from Roussel's book on understanding the rheology of concrete [31], Billberg's doctoral thesis on influence of thixotropy and structural behavior of SCC at rest on the formwork pressure [6], and Assaad's doctoral thesis on influence of thixotropy on formwork pressure [13].

2.3.1 Introduction

Concrete has been used extensively since the beginning of the twentieth century. However, the understanding its behavior in the fresh state only started in the last 50 to 60 years due to the advancement of the modern science of rheology and the development of technology. The research on the rheology of fresh concrete focusses mainly on the ability to correctly measure and quantify the rheological properties, to understand the correlation between mix components (and their proportions) and rheological properties in the fresh state, and the ability to predict whether or not

a given concrete will correctly fill a given formwork. A summary of different rheological behaviors with an emphasis on the behavior seen in the cementitious materials and types of interactions within material responsible for these rheological behaviors are discussed below.

In the case of simple materials like the solid crystals made of identical atoms arranged in the symmetric and periodic positions, the interactions between the neighboring atoms happen due to the van der Waals forces, ionic or covalent forces and these interactions vary with respect to the distance between the atoms. Each atom is in an equilibrium position corresponding to minimum potential energy. As a result, each atom is in a minimum potential energy well, and a certain force needs to be applied for the atom to escape the well. So a when a low stress is applied, the atom displaces slightly along its minimum potential well. This small motion of the atoms manifests as deformation of the material as a whole. When the force is released, the atom falls back to the minimum potential well. This explains the elastic behavior of the material in the limit of small deformations. When a sufficiently large force is applied, the atom can jump out of the potential well thereby resulting in dislocation (plastic behavior) or breakage (failure). In simple materials, it is possible to correlate microscopic behavior to the phenomenon observed on the macroscale. In the case of materials with densely packed atoms (similar to crystalline solids) but without a periodic arrangement of atoms, it is harder to correlate the local displacements of atoms to macroscopic deformations because the stress distribution along the structure is not known.

Similar to the analysis done in the case of pure solids, the macroscopic deformations in simple colloids made of mesoscopic elements dispersed in fluids with colloids in crystalline order can be explained based on the potential energy between the mesoscopic elements. However, in more complex materials like concrete, wide range of particles (colloidal particles and coarse grains in a liquid solution). The structure is disordered and has multiple types of interactions resulting from

the wide range of particles. This makes it difficult for establishing a relationship between the local and macroscopic behavior.

For fluids under usual conditions, the flow rate plays a critical role in the rheological behavior description. For Newtonian fluids, the shear stress is proportional to the shear rate. The ratio of the shear stress to shear rate is defined as the viscosity of the material. Similar to the simple solids, the macroscopic behavior in a simple fluid can be related the element packing and the interactions with their neighbors.

For suspensions, the fluid layers follow more complex paths compared to pure liquids due to the presence of elements. This results in larger viscous dissipation forces for a larger concentration of elements. The effective behavior of the suspensions is complex because the source of viscous dissipation could be due to the friction between the particles in contact (solid) or it could be due to the hydrodynamic dissipations in interstitial liquid (fluid).

For some fluids, the apparent viscosity varies with shear rate and flow history. These fluids are classified as non-Newtonian. This is the characteristic of suspensions with asymmetrical elements that can change their orientation or shape during the flow or objects developing mutual interactions which vary with the flow history. The asymmetrical elements align themselves along the flow thereby reducing the apparent viscosity of the fluid. Such fluids are identified as shear-thinning (viscosity decreases with shear rate). In some fluids, the alignment takes some time to develop, and such fluids are called thixotropic. Both shear thinning and the thixotropy originates from same physical effect but are associated with different mechanical effects.

Some fluids behave both as solid and liquid depending on the amount shear stress applied. Such fluids are identified as yield stress fluids. These fluids behave as elastic solid under a critical stress

value, i.e., the yield stress and about that it behaves as a viscous liquid. In the solid regime, the mechanical approach developed for the simple solids can be used to understand the physical origin of the rheological properties. However, no such relation can be established for the liquid regime.

Most of the yield stress fluids exhibit thixotropic properties. In the solid regime, the thixotropic effects are characterized based on the increase in elastic modulus or increase in apparent yield stress with time. This increase in case of simple colloids can be correlated to the increasing in jamming and interaction strength. In the case of the liquid regime, thixotropy can be characterized based on the decrease in the apparent viscosity with time or decrease in shear stress when the shear rate is imposed. These effects are associated with the fact there is a steady state structure corresponding to the shear rate applied and the material takes a certain time to get to the steady state. This manifests as thixotropy in the material. For simple suspensions of attractive particles, this effect can be correlated to the breakage of a network of linked particles into smaller flocs. For more complex materials with a significant fraction of colloidal particles, the stress needed to change from solid to the liquid regime and the stress needed to maintain the flow are different. This gives rise to the concept of static and dynamic yield stress.

Concrete can be classified as complex suspension. The behavior of concrete in the fresh state is strongly effected by time. When left at rest, the consistency of concrete increases with time. This increase is partly due to the reversible effects (thixotropic), and so these effects can be eliminated by shearing the material (for example by remixing using a concrete mixer). The increase in consistency is also partly due to the hydration process which is irreversible, and these effects contribute to the long-term evolution of concrete properties in the hardened state. The methods for the measurement of properties of the thixotropic yield stress fluids are presented in the following paragraphs.

2.3.2 Measurement techniques for thixotropic yield stress fluids

Thixotropic yield stress fluid properties are dependent on the flow history, so it is difficult to express its characteristics in terms of fundamental and absolute terms.

2.3.2.1 Thixotropic Loop

In this experiment, the material is subjected to a continuously increasing and decreasing shear rates. The hysteretic response indicates the dependence of material behavior on shear history. The area under the thixotropic loop is used as a measure of thixotropy. However, throughout the shear history during the test, the material structure evolves in a way which depends complexly on the shear ramp rate used and only qualitative results can be obtained from this tests.

2.3.2.2 Creep Tests

Creep tests consist of applying series of constant shear stresses (or shear rates) over a long period after pre-shearing the material. The dynamic yield strength values can be obtained from creep tests when a series of shear stresses are applied. So quantitative outputs can be obtained from this test. However, the test takes a long time and do not provide a lot of data. The data obtained can be effected by shear banding that could happen in the rheometer, so an accurate understanding the test setup, the assumption used for the determination of the rheology parameters and prior determination of the critical shear rate in a controlled stress mode are needed to get the accurate results from his test.

2.3.2.3 Static Yield Stress Measurements

At low shear values, the shear stress roughly increases linearly with shear strain (elastic region). At the yield strain value, the maximum shear stress is reached known as the static yield stress

value. To obtain the static yield stress gain over time, this test has to be repeated for various resting times, and each experiment provides one value of yield strength and the corresponding time. Because the static yield strength value is highly dependent on the flow history, it is crucial to obtain a well-defined aging solid state of the material. In some systems, the elastic modulus gain over time can be measured since the elastic modulus gain is quantitatively similar to the yield stress gain. This approach is an advantageous measurement of elastic modulus can be done without disturbing the material. However, in the case of cement based materials, this approach cannot be used. Because the origin of elastic modulus and yield stress are different and also have different time evaluations. Elastic modulus increase is linked to the early age of hydration and yield stress gain linked to the rearrangements of the colloidal network.

CHAPTER 3

EXPERIMENTAL PROGRAM

The experimental program in this project was designed to measure the formwork pressure and pressure decay accurately and to understand the mechanism behind the pressure variation with different parameters which will be discussed in detail in this section and section CHAPTER 4.

3.1 Materials

ASTM C 150: "Standard Specification for Portland Cement" Type I/II ordinary Portland cement and ASTM C 618: "Standard Specification for Coal Fly Ash and Raw or Calcined Natural Pozzolan for Use in Concrete" Type C fly ash were used for the study. The physical and chemical characteristics of the cement and fly ash are shown in **Table 1**.

Table 1 Chemical and physical properties of fly ash and cement

Materials/ Properties	Fly Ash	Cement
SiO_2	38.04	19.4
Al_2O_3	18.81	5.4
Fe_2O_3	5.81	2.4
SO_3	1.08	2.7
CaO	25.41	63.5
MgO	4.94	3.3
Na_2O	1.49	--
K_2O	0.71	--
C_3S	--	61.6
C_3A	--	9.9
Limestone	--	3.2
$CaCO_3$ in Limestone	--	93
Total Alkali	1.96	0.2
Moisture	0.06	--
Loss on Ignition	0.55	2.2
Fineness, % retained on #325	14.73	6.7
Density	2.90	3.15

Continuously graded crushed limestone with the maximum aggregate size of 1 in. (25.4 mm) was used. The specific gravity and absorption capacity of the coarse aggregate were determined as per

ASTM C127 – 15: "Standard Test Method for Relative Density (Specific Gravity) and Absorption of Coarse Aggregate." The sieve analysis data and the physical properties of the coarse aggregates are shown in **Table 2** and **Table 4** respectively. The coarse aggregate with different gradation and maximum aggregate size were used for studying the effect of aggregate size on the formwork pressure decay. The details of these gradations are provided in the section 0.

Table 2 Particle size distribution for limestone

Sieve Size	Cumulative Amount Passing (%)
1 in	100
3/4 in	77
1/2 in	29
3/8 in	12
No. 4	1
No. 16	0
Pan	0

The size distribution of fine aggregate was determined as per ASTM C136 / C136M – 14: "Standard Test Method for Sieve Analysis of Fine and Coarse Aggregates." The specific gravity and absorption capacity of the sand were determined as per ASTM C128 – 15: "Standard Test Method for Relative Density (Specific Gravity) and Absorption of Fine Aggregate." The physical properties of the sand are shown in **Table 3** and **Table 4** respectively.

Table 3 Particle size distribution for natural sand

Sieve Size	Cumulative Amount Passing (%)
No. 4	92
No. 8	85
No. 16	77
No. 30	62
No. 50	23
No. 100	0
No. 200	0
Pan	0

Table 4 Specific gravity and water absorption for aggregates

Property	Crushed Limestone	Natural Sand
Specific Gravity (SSD)	2.57	2.60
Specific Gravity (OD)	2.51	2.56
Absorption (%)	2.70	1.50

Polycarboxylate polymer (Sika ViscoCrete 2100) based high range water reducing admixture (HRWR) that meets the requirement for ASTM C494 / C494M – 16: "Standard Specification for Chemical Admixtures for Concrete" Types A and F was used. Viscosity modifying admixture (MasterMatrix VMA 362) that meets ASTM C 494/C 494M requirements for Type S was also used to prevent the mix from segregating. Synthetic Macro Fiber Reinforcement (STRUX 90/40) were also used to study the effect of fibers on rheology and formwork pressure decay.

3.2 Mixing Procedure

Concrete pan mixer (shown in **Figure 1**) was used for mixing of concrete. Consistent mixing procedure was followed for all the mixes (if any exceptions, then the adapted mixing procedure is mentioned in the particular subsection in results and discussion section). The pan was wetted with water, and the excess water was wiped off using paper towels. All the aggregate was added to the pan, and approximately half of the mix water was added to the aggregate and mixed for 1 minute. Then the cementitious material was added to the pan followed by the remaining water. After mixing for 2 minutes, the mixer was stopped and left to rest for 1 minute. The chemical admixture (HRWR or VMA) was added to the pan, and the concrete was re-mixed for another 2 minutes. When both HRWR and VMA were used, the HRWR was added to the mix water, and the VMA was added to the concrete after the resting period. When the fibers were used, the fibers were added to the pan along with the aggregate to ensure proper dispersion of the fibers.

Figure 1 Concrete pan mixer

3.3 Slump Flow Test

The slump flow test was performed to assess the flowing ability of SCC and mortar. The test was performed as per ASTM C1611 / C1611M – 14: "Standard Test Method for Slump Flow of Self-Consolidating Concrete." The damp slump cone (as shown in **Figure 2**) was placed on the damp level surface (level base plate) such that the smaller opening of the cone was facing down. The cone was filled with concrete or mortar using a scoop. The surface of the concrete was levelled and the cone was lifted up vertically. The spread of the concrete or mortar was measured, and the average spread of the concrete or mortar was reported as slump flow.

Figure 2 Slump flow test

3.4 Pressure Sensors and Test Setup

Two different flush diaphragm pressure sensors were used in the current project. One type of the sensors used had a pressure range of 0-100 psi (Omega PX 102 series), and the other sensors had a pressure range of 0-15 psi (TE Connectivity 82 CV series). P3 Strain Indicator and Recorder, NI compactDAQ and NI 9237 modules were used for acquiring the pressure data. The data acquisition systems and the pressure sensors used are shown in **Figure 3**, **Figure 4**, and **Figure 5**.

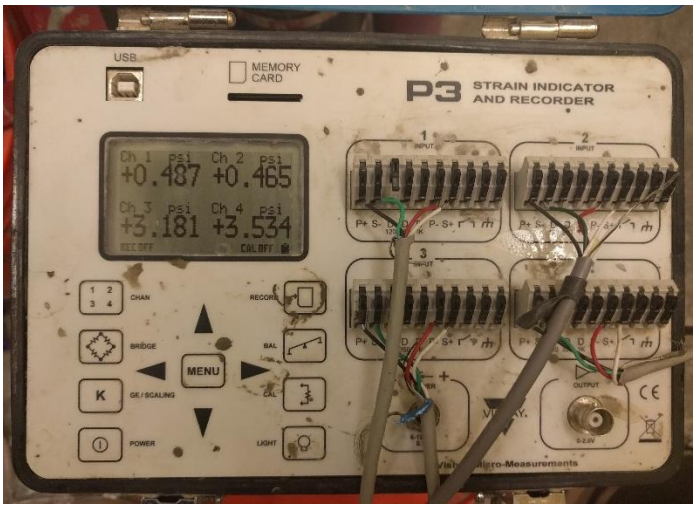

Figure 3 P3 Strain Indicator and Recorder

Figure 4 NI compactDAQ and NI 9237 module

Figure 5 Pressure sensors: 0 – 15 psi (left), 0 – 100 psi (right)

Three PVC pipes with different dimensions were used to make the formwork columns. The schematic of the formworks is shown in **Figure 6**. The black dots indicate the location of the sensors. Form1 had dimensions of 36in. length and 10in. diameter, Form2 had dimensions of 24in. length and 6in. diameter and Form3 had dimensions of 60in. length and 4in. diameter.

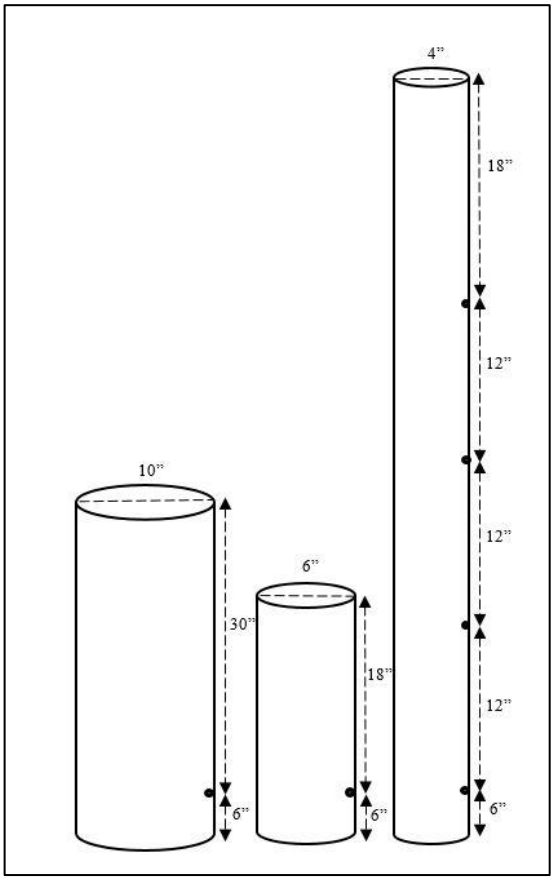

Figure 6 Schematic of the three formworks Form1, Form2, and Form3 (from left to right) along with the sensor location used

3.5 ICAR Rheometer

ICAR rheometer was used to characterize the rheological properties of fresh concrete and mortar. Stress growth tests were performed to determine static yield stress gain over time, and flow curve tests were performed to determine the dynamic yield stress and viscosity gain over time for concrete and mortar. Stress growth test involved rotating the vane at a low and constant speed (0.025 rev/sec) and monitoring the buildup torque. The maximum torque corresponded to the torque beyond which the material starts yielding. So the maximum torque value was used to

compute the static yield stress value. Based on the maximum torque value and geometry vane used the ICAR rheometer software computed the static yield stress value using the following Equation (19). Stress growth test is highly dependent on the history of the sample. So a new sample was used for each static yield stress data point for a given concrete/mortar mix. For the flow curve test, the material first sheared to breakdown the thixotropic buildup in concrete/mortar by rotating the vane at the maximum speed (0.50 rev/sec) for 20 seconds. Then the vane speed decreased gradually from 0.50 rev/sec to zero in prescribed number of steps (seven steps in the present case). During each of these steps, the average speed and the corresponding torque were recorded by the ICAR rheometer, and the dynamic yield stress value was determined using the Equation (19) and assuming that the concrete/mortar tested followed Bingham model behavior. The ICAR test setup is shown in **Figure 7**.

$$\tau = \frac{2T}{\pi D^3 \left(\frac{H}{D} + \frac{1}{3}\right)} \tag{19}$$

Where

τ is the yield stress

T is the torque

D is the vane diameter

H is the height of van

Figure 7 ICAR rheometer test setup

3.6 Temperature Sensors

The temperature changes of concrete (mortar or cement paste) within the formwork were measured using type T thermocouple (temperature range -250° to 350°C) and thermocouple data logger (USB TC-08) (shown in **Figure 8**). The temperature measurements were carried out to measure the rate of hydration and to understand the mechanisms behind pressure decay.

Figure 8 Data Logger (on left) and type T thermocouple (on right)

CHAPTER 4

RESULTS AND DISCUSSIONS

4.1 Effect of Mix Design Parameters

4.1.1 Effect of w/cm

Effect of water to cementitious ratio (w/cm) on formwork pressure change over time was studied by varying the w/cm from 0.37 to 0.41 (by weight) in concrete. The effect was also studied using mortar mix with w/cm 0.38 and 0.46 and cement paste with w/cm varying from 0.4 to 0.47. The mix proportions used in this study are shown in **Table 5**. The mixes were cast using Form1, Form2, and Form3. The schematic of the forms is shown in **Figure 6**. To maintain the same conditions like temperature and humidity, both the concrete mixes were cast on the same day (time difference of less than an hour). Same was the case with mortar and cement mixes. The lateral pressure was measured over time using Omega PX 102 series pressure transducers and 'P3 Strain Indicator and Recorder'. The relative lateral pressure changes in Form1 and Form3 (for mixes SCC1, SCC2, M1, M2, C1, and C2) are shown in **Figure 9**, **Figure 10**, and **Figure 11**. The static yield strength data for mixes M1 and M2 are shown in **Figure 12**.

Table 5 Proportions of the evaluated mixtures

Materials	Units	SCC1	SCC2	M1	M2	C1	C2
Type I/II OPC	lb/ft^3	24.1	23.6	53.3	49.8	87.0	79.2
Class C Fly ash	lb/ft^3	7.3	7.2	--	--	--	--
Water	lb/ft^3	11.5	12.5	20.1	22.8	34.8	37.2
Sand	lb/ft^3	52.6	51.6	62.6	58.6	--	--
Limestone	lb/ft^3	49.2	48.2	--	--	--	--
Water to cementitious ratio	--	0.37	0.41	0.38	0.46	0.40	0.47
High Range Water Reducing admixture	Ml	26	26	--	--	--	--
Target slump flow	In	22	26	22.5±0.5	39	--	--

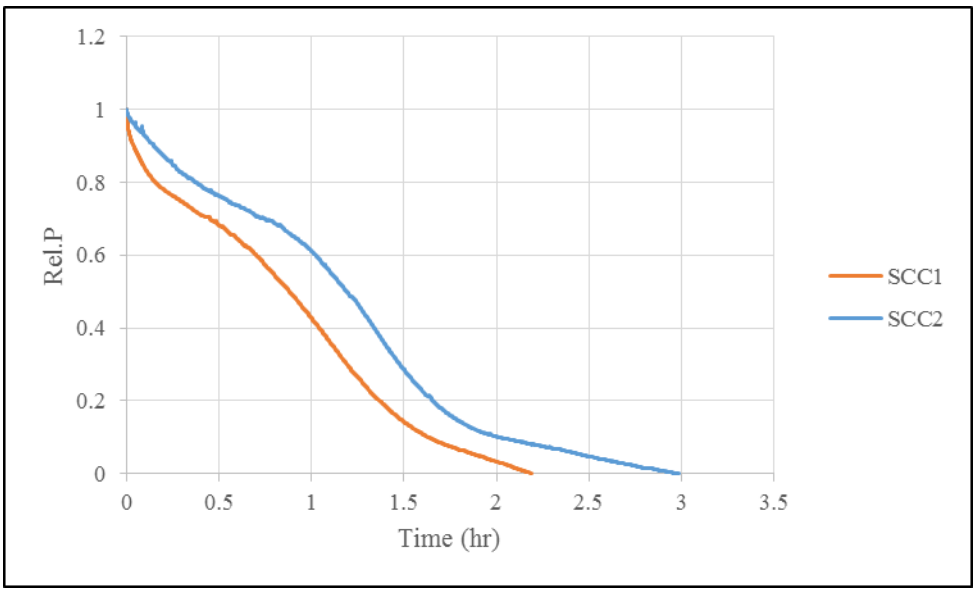

Figure 9 Relative formwork pressure (w.r.t max. hydrostatic pressure) variation with time for Form1

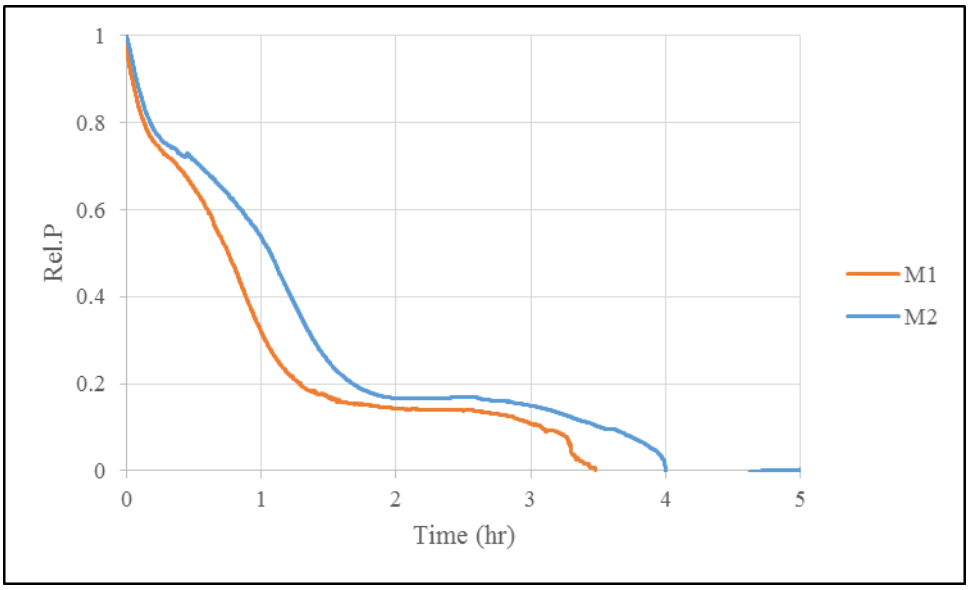

Figure 10 Relative formwork pressure (w.r.t max. hydrostatic pressure) variation with time for Form3 at 4.5ft depth

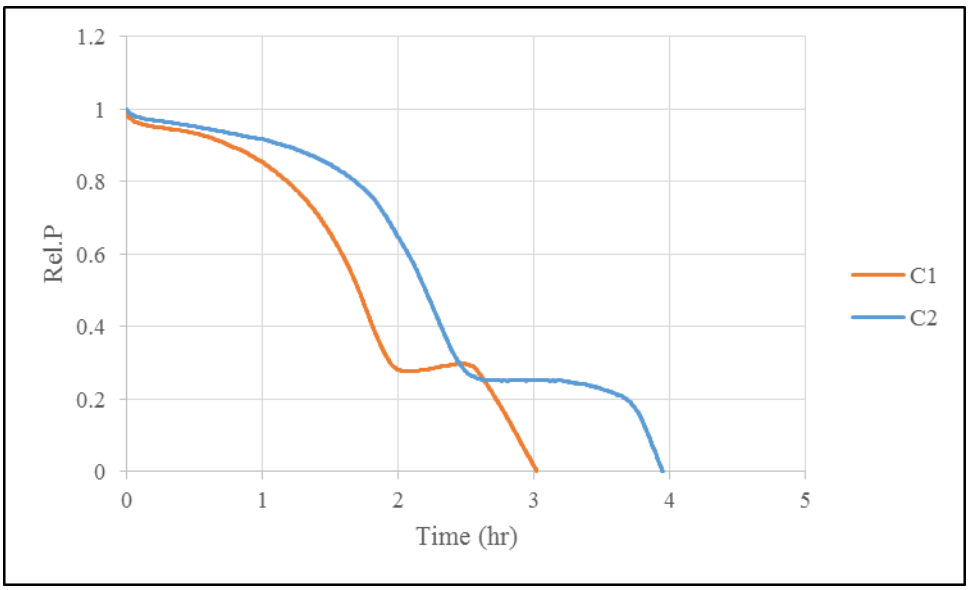

Figure 11 Relative formwork pressure (w.r.t max. hydrostatic pressure) variation with time for Form2

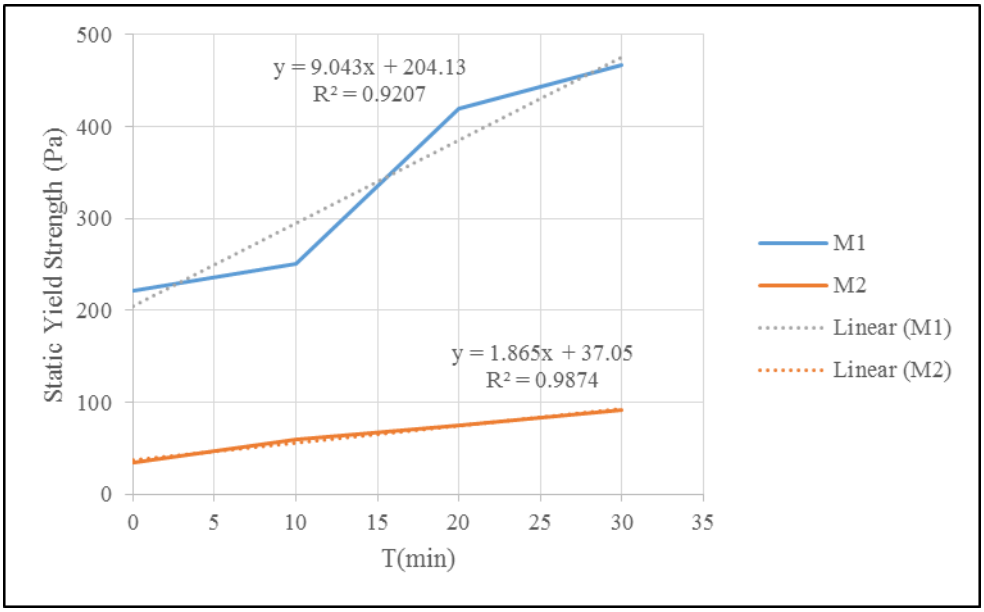

Figure 12 Static yield strength variation with time measured using ICAR rheometer

Figure 9 is the formwork pressure decays for mixes SCC1 and SCC2 cast in formwork of same dimensions on the same day (approximately thirty minutes apart). Similarly, **Figure 10** and **Figure 11** are for mixes M1, M2, and C1, C2 respectively. From all the three figures, it is clear that the

pressure decay is faster for mixes with lower water to cementitious ratio (w/cm). From **Table 5**, the slump flow values are also lower for mixes with lower w/cm indicating lower workability. From **Figure 12**, the static yield strength values are higher, and the gain is also faster (higher value of slope) for mix M1 compared mix M2 (has higher w/cm ratio). Higher yield strength values for mixes with lower w/cm ratio indicates that the material can support its weight better thereby applying less stress on the formwork. Faster yield strength gain in lower w/cm ratio mix also explains the faster pressure decay. The faster decay in lower w/cm ratio mixes is the opposite of what was observed by Khayat et al. [16]. The authors considered that it is probably due to the greater High Range Water Reducing (HRWR) admixture demand in the low w/cm ratio mixes thereby reducing fluidity loss with time and buildup in cohesiveness. However, in the present case, the HRWR dosage is kept constant between the mixes under comparison.

4.1.2 Effect of addition of fly ash

Effect of Fly Ash (FA) was studied by making two mixes (M1 and M2). Mix 1 (M1) was made using Type I/II Ordinary Portland Cement (OPC). Mix 2 (M2) was made using both OPC and FA. For M2, 30% by volume of OPC for M1 was replaced with FA. The mix proportions and the slump flow values for the mixes are shown in **Table 6**.Form1 and Form2 were used for this study. The schematic of the formworks are shown in **Figure 6**. Both mixes M1 and M2 were made on the same day (time difference of less than an hour) to make sure the environmental conditions (temperature and humidity) stay the same. The lateral pressure was measured over time using Omega PX 102 series pressure transducers and 'P3 Strain Indicator and Recorder'. The relative lateral pressure changes in Form1 and Form2 (for mixes M1 and M2) are shown in **Figure 13** and **Figure 14**. The static yield strength data for mixes is shown in **Figure 15**.

Table 6 Proportions of the evaluated mixtures

Materials	Units	SCC1	SCC2
Type I/II OPC	lb/ft^3	33.2	23.6
Class C Fly ash	lb/ft^3	--	7.2
Water	lb/ft^3	12.5	12.5
Sand	lb/ft^3	51.5	51.5
Limestone	lb/ft^3	48.2	48.2
Water to cementitious ratio	--	0.38	0.41
High Range Water Reducing Admixture	Ml	36	36
Target slump flow	In	24	28

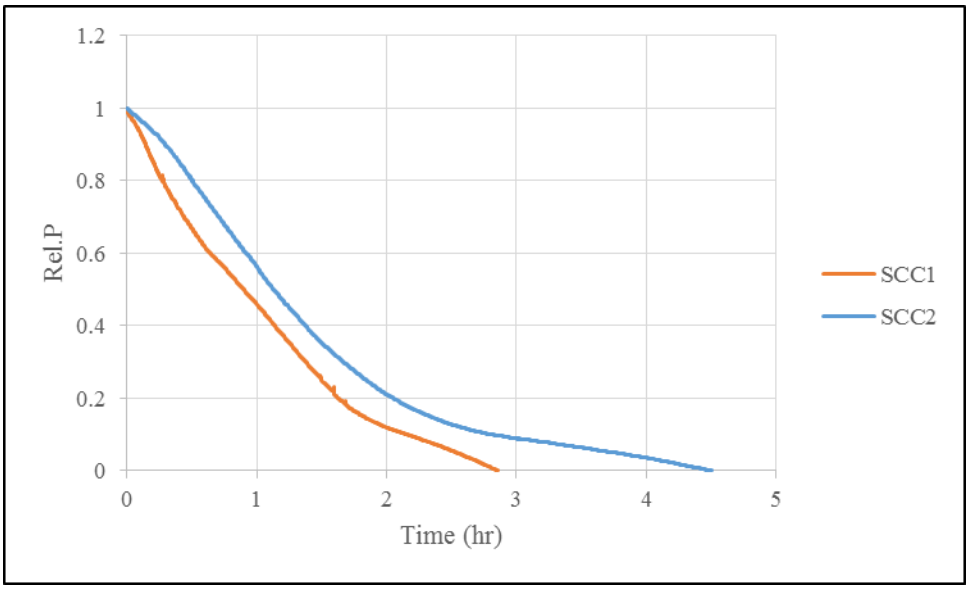

Figure 13 Relative formwork pressure (w.r.t max. hydrostatic pressure) variation with time for Form1

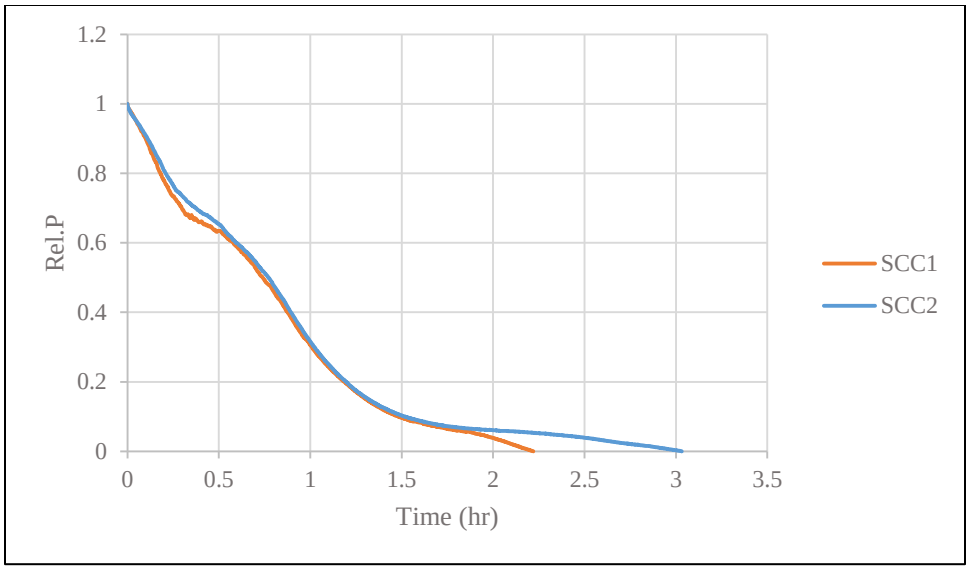

Figure 14 Relative formwork pressure (w.r.t max. hydrostatic pressure) variation with time for Form2

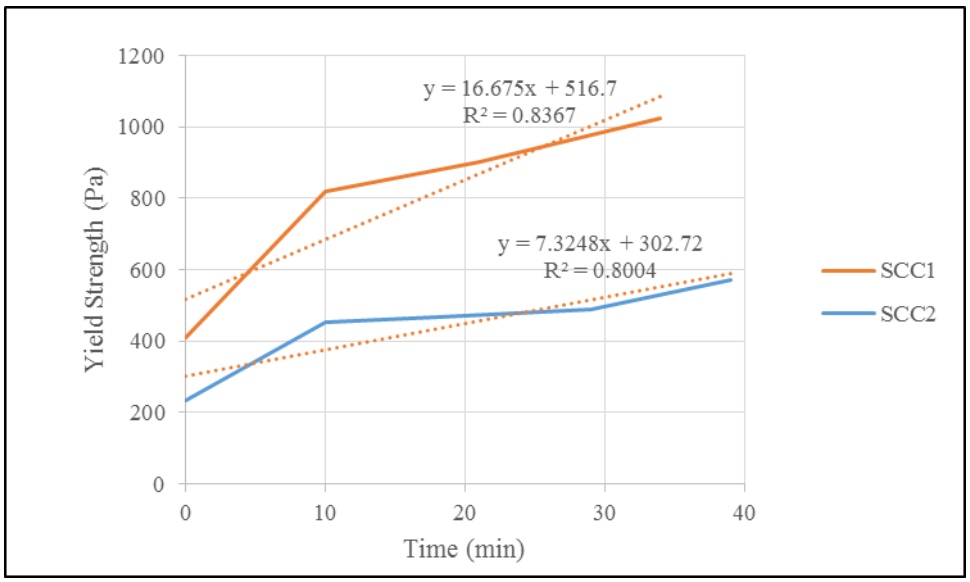

Figure 15 Static yield strength variation with time measured using ICAR rheometer

Figure 13 is the formwork pressure decays for mixes SCC1 and SCC2 cast in formwork of same dimensions on the same day (approximately one hour apart). The pressure decay is faster for a mix

without fly ash (SCC1). From **Table 6**, the slump flow values are also lower for SCC1 mix indicating lower workability. From **Figure 15** and **Figure 13**, the static yield strength values are higher, and the gain is also faster (higher value of slope) for mix SCC1 compared to mix SCC2 (contains fly ash). Higher yield strength values for SCC1 indicates that the material can support its weight better thereby applying less stress on the formwork. Faster yield strength gain in SCC1 mix also explains the faster pressure decay. The difference in pressure decay between the two mixes is less evident in the case of Form2 as shown in **Figure 14**. This could be due to the arching effect which is explained in the effect of formwork dimensions section [Section 0]. The pressure decay behavior observed with fly ash is different from the behavior mentioned in literature review section. This is probably due to the difference in the CaO content (Assaad [6]) and the difference in particle size (Burak et al. [5]).

4.1.3 Effect of aggregate properties

4.1.3.1 Moisture content

Natural sand with different moisture contents was used as fine aggregate in the present study. Two mortar mixes with same mix proportions were prepared. The aggregate was oven dried and sieved before the test to maintain the consistent gradation for both mixes. The oven dried and sieved aggregate was directly used for one of the mixes (M1). For the other mix (M2), the oven dried and sieved aggregate was soaked in the mix water for 24 hours. For mix M1, the total water added while mixing was water needed to account for the reported w/cm ratio and the water needed for the aggregate to reach to surface saturated condition (SSD). For mix M2, the aggregate was presoaked in the total water needed for the mix, i.e., water needed to account for the reported w/cm ratio and the water needed for the aggregate to reach to surface saturated condition (SSD). So the

mix proportions were kept same for both mixes. For the presoaked aggregate mix, mixing procedure adopted was slightly different compared to one mentioned in Section 0. Because the aggregate is already soaked in the mix water, it was mixed using a pan mixer for one minute. After that the cement was added to the pan and mixed for two minutes, the mixer was then stopped and left to rest for one minute. The mortar was remixed for one minute before pouring into the formwork. The mix proportions used in this study are shown in **Table 7**. The formwork pressure decay data collected using Form2 are shown **Figure 16**.

Table 7 Proportions of the evaluated mix

Materials	Units	Mix
Type I/II OPC	lb/ft^3	33.5
Water	lb/ft^3	17.8
Sand	lb/ft^3	73.2
Water to cementitious ratio	--	0.53

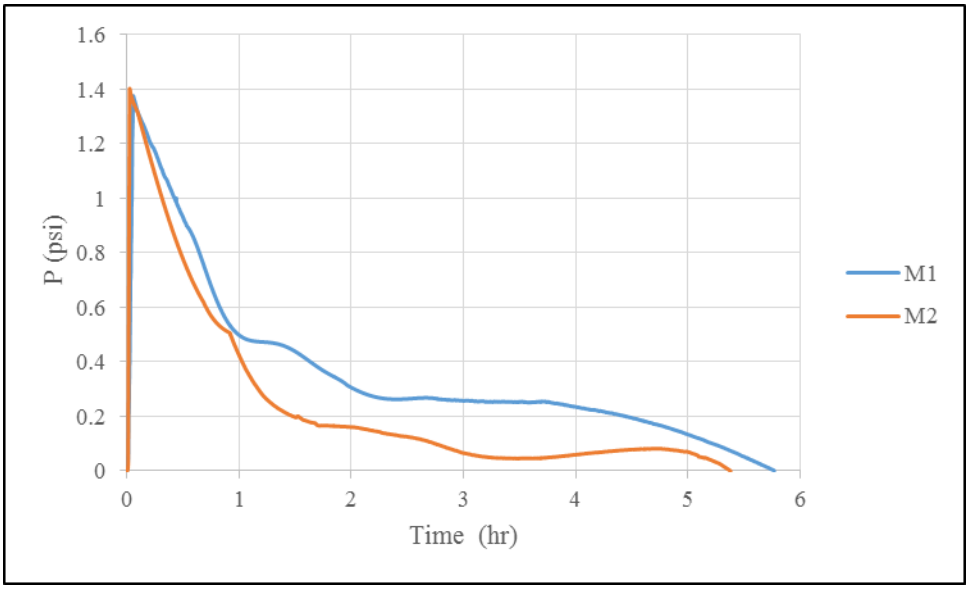

Figure 16 Relative formwork pressure (w.r.t max. hydrostatic pressure) variation with time in Form2

Figure 16 is the formwork pressure decays for mixes M1 and M2 cast in formwork of same dimensions on the same day (approximately one hour apart). The pressure decay is slightly faster in mix M2 (with pre-soaked aggregate) compared to M1 (oven dry aggregate). The pressure cancellation time, i.e., the time at which the pressure drops to zero (T_c) is also lower for M2 compared to M1. These results indicate that in the case of oven dry aggregate, not all the extra water added along with the mix water during mixing was absorbed by the aggregate thereby increasing effective water to cementitious ratio. As a result, the pressure decay is slower in the mix M1.

To check the time taken for the aggregate to absorb the water to get to SSD condition following investigation was done. During this investigation, the absorption rate of the aggregate was studied. For the coarse aggregate (limestone), the aggregate was washed thoroughly on 4.75 mm sieve. Then the aggregate was oven dried for 24 hours. The oven dried aggregate was sieved again to remove any fines left (any aggregate finer than 4.75 mm). This aggregate was then cooled to room temperature. The aggregate was submerged in water bucket using a sieve basket and the gain in submerged mass of the aggregate over time was recorded. The loss of moisture due to evaporation can increase the submerged mass of the aggregate. So the water bucket was covered to reduce the evaporation losses. Based on the absorption rate experiments conducted in the first few trials, it was observed that even after thoroughly washing the aggregate there were still some fines left (shown in **Figure 17**). So the aggregate was soaked in water for a week to get rid of these fines. Then it was oven dried for three days before sieving and using for the absorption tests (the weight of the aggregate was constant after oven drying for three days). For the fine aggregate (natural sand) similar procedure was adopted. The aggregate was sieved to remove the aggregate finer than No. 16 sieve (1.19 mm), and the aggregate was submerged in the water using the Polypropylene

mesh (0.53 mm x 0.68 mm nominal dimension). The absorption rate over time for the aggregate samples measured is shown in **Figure 18** and **Figure 19** below.

Figure 17 Fines found at the bottom of the bucket after soaking the sieved aggregate in water for a week

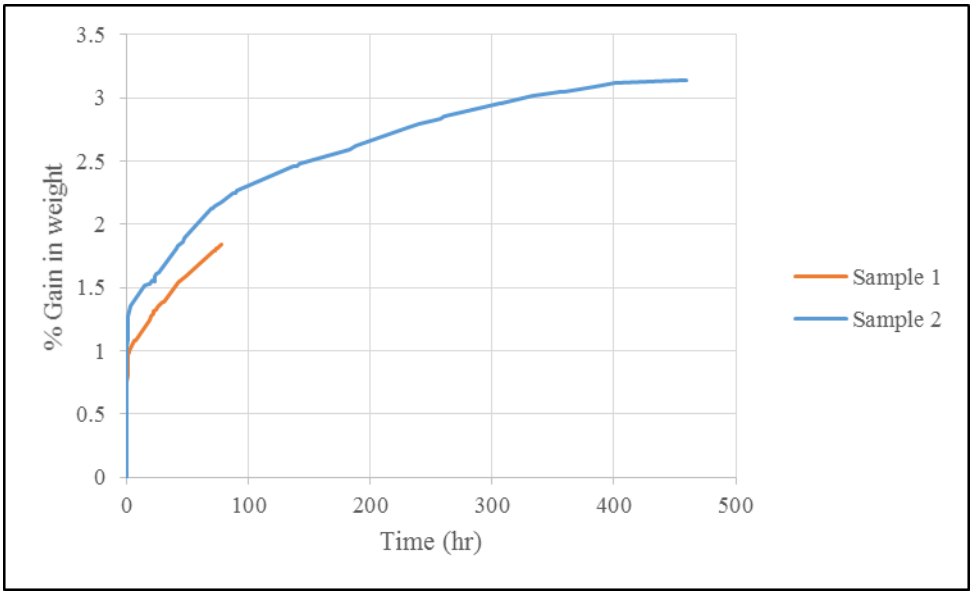

Figure 18 Absorption rate over time for limestone aggregate samples

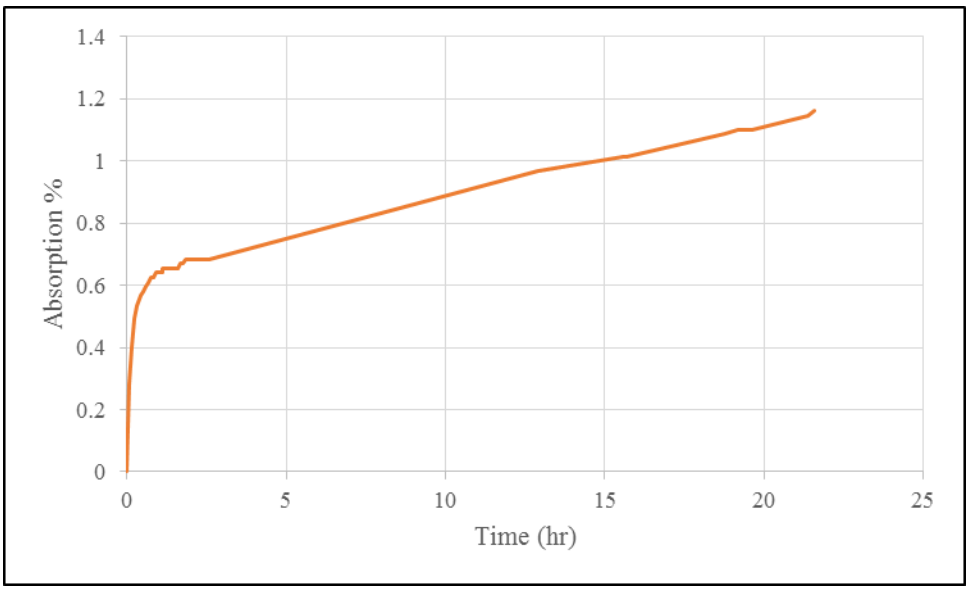

Figure 19 Absorption rate over time for fine aggregate (sand) samples

From the absorption results for the aggregates, it is clear that all the moisture absorption does not happen within the first 24 hours. So soaking the aggregate for the 24 hours is not enough to achieve SSD condition at least for the aggregates tested (Limestone and Natural Sand). Even though the evaporation losses were minimized by covering the water, there may have been some evaporation especially in the case of limestone sample 2 (results are shown in **Figure 18**) where the test was conducted over 20 days. At the start of the test, after the sample was submerged in the water, it had to be agitated to remove the air bubbles. The need for agitation and the rapid rate of absorption in the first few minutes may have resulted in inaccurate measurements in first 5 minutes of the data collected.

Despite these limitations, it is clear that the moisture absorption into the aggregate for it to reach SSD condition does not happen instantaneously. In fact, it does not seem to happen even within 24 hours as mentioned in the standards ASTM C127 – 15: “Standard Test Method for Relative

Density (Specific Gravity) and Absorption of Coarse Aggregate" and ASTM C128 – 15: "Standard Test Method for Relative Density (Specific Gravity) and Absorption of Fine Aggregate". So it can be said that the significant amount of the extra water added for the aggregate absorption in case of mix M1 (in **Figure 16**) was available as free water to increase the workability of the mix. Alhozaimy [32] observed that the absorption capacity of the aggregate is different in the concrete environment compared to when measured in pure water. The author's results indicated that limestone aggregates used had an absorption capacity of 1.3–1.9% by weight when measured in water. However, when the same amount of water is added to the concrete for aggregate absorption only 75% of that water gets absorbed, and the remaining 25% will add to the free water, thus increasing the effective w/c ratio thereby resulting in increased workability. This may also have contributed to slower pressure decay in mix M1.

4.1.3.2 Aggregate size

The effect of aggregate size on the formwork pressure behavior of SCC was studied by making two concrete mixes with same mix proportions. For each mix, different coarse aggregate sizes were used. The particle size distribution of the aggregates used and the mix proportions are shown **Table 8** and **Table 9** respectively. Form1 was used to measure the pressure decay, and the data is shown in **Figure 20**.

Table 8 Particle size distribution of the coarse aggregate

Mix	**A**	**B**
Sieve Size	**% Retained on each sieve**	
0.75 in	5.0	0.0
0.5 in	40.0	0.0
0.375 in	42.5	5.0
No.4	7.5	57.5
No.16	5.0	37.5

Table 9 Proportions of the evaluated mixtures

Materials	Units	Mix Proportions	
Type I/II OPC	lb/ft^3	32.8	
Water	lb/ft^3	53.8	
Sand	lb/ft^3	48.7	
Limestone	lb/ft^3	11.7	
Water to cementitious ratio	--	0.36	
High Range Water Reducing Admixture	ml	83.0	
Viscosity Modifying Agent	ml	100.0	
--	--	**Mix A**	**Mix B**
Target slump flow	in	28.5	27.0

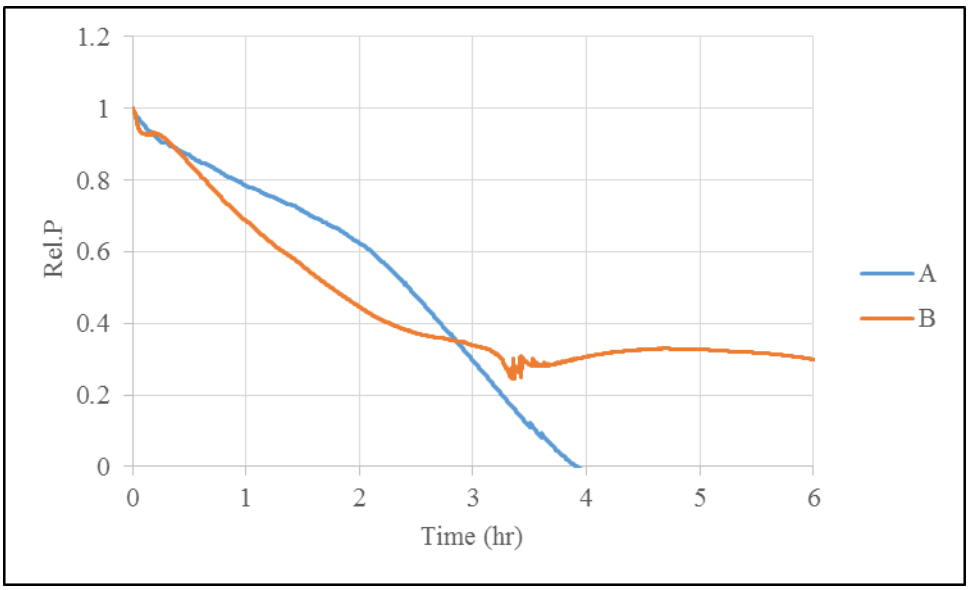

Figure 20 Relative formwork pressure (w.r.t max. hydrostatic pressure) variation with time measured using Form1

From the pressure decay data in **Figure 20**, the pressure decay is faster for mix B. From **Table 8**, mix B has the maximum aggregate size (MAS) of 0.375 inches and mix A has MAS of 0.75 inches. The pressure decay seems to be faster in the mix with smaller aggregate. This could be because as the aggregate size decreases the surface area that needs to be coated with the cement paste increases

thereby decreasing the amount of paste available for the workability of the mix. As a result, Mix B has lower slump flow value as shown **Table 9** compared to Mix A. As a result, the concrete prepared using Mix B can retain its shape better and support its weight better thereby applying less stress on the formwork.

4.1.3.3 Aggregate content

To study the effect of the aggregate content two different experiments are conducted. In one experiment, the fine aggregate content was varied for the mortar mixes keeping everything else constant. In the other experiment, the pressure decay data for concrete, mortar, and cement paste mixes were compared.

For the first experiment, three mortar mixes with different aggregate contents were studied. The mix proportions used are shown in **Table 10**. Form3 was used to measure the formwork pressure decay. The three mixes were made on consecutive days, and the weather conditions were more or less same when the mixes were cast. The static yield stress data was also measured using the ICAR rheometer. The pressure decay data and static yield stress change over time are shown in **Figure 21** and **Figure 22** respectively.

Table 10 Proportions of the evaluated mixtures

Materials	Units	M1	M2	M3
Type I/II OPC	lb/ft^3	50.0	43.2	39.8
Water	lb/ft^3	22.8	19.8	18.2
Sand	lb/ft^3	58.6	68.8	78.0
Water to cementitious ratio	--	0.46	0.46	0.46
Sand to cement ratio (by vol.)		1.5	2.0	2.5
Target slump flow	in	37.75±1.25	30.25±0.25	25.5±1.5

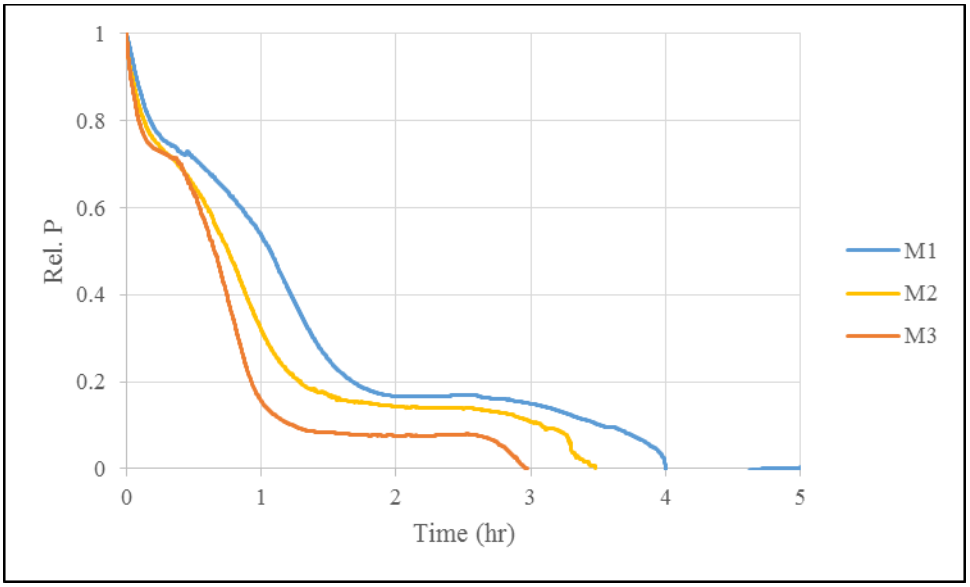

Figure 21 Relative formwork pressure (w.r.t max. hydrostatic pressure) variation with time measured using Form2 at 3.5 ft depth

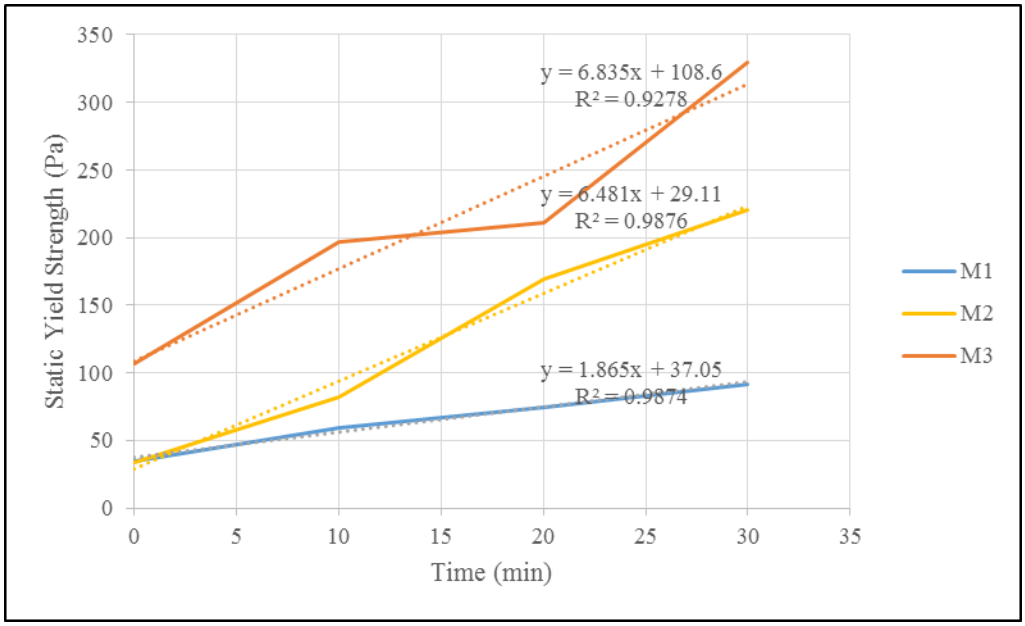

Figure 22 Static yield stress change over time for mixes M1, M2, and M3

From the results in **Figure 21**, as the aggregate content increases (aggregate to cement ratio by volume from 1.5 to 2.5) the pressure decay is faster. The static yield stress data in **Figure 22** also shows that the static yield is higher and the gain is faster in mix M3 compared to mixes M1 and M2. The increase in the rate of pressure decay and an increase in the yield stress are caused due to the higher degree of friction and interlock of solid particles. This is also the reason for lower workability (slump flow) as the aggregate content is increased for the mixes in **Table 10**. As per Omran et al. [10] and Amziane et al. [11], the reason for the faster pressure decay also seem to be due to the increase in the rate of precipitation of hydration products as the fine aggregate offers numerous nucleation sites and the accelerated rate of stiffening of concrete due to the concentration of the pore solutions between the closely packed aggregate particles.

For the second experiment, three mixes concrete, mortar, and cement paste were considered. None of these mixes were made on the same day. These mixes are compared purely to talk about the effect the presence/absence of the aggregate has on pressure decay behavior over time. The pressure decay considered for all the three mixes are using Form1. The mix proportions are shown in **Table 11**. The pressure decay data is shown in **Figure 23**.

Table 11 Proportions of the evaluated mixtures

Materials	Units	A	B	C
Type I/II OPC	lb/ft^3	33.2	43.2	80.3
Water	lb/ft^3	12.5	19.8	36.9
Sand	lb/ft^3	51.5	68.8	--
Limestone	lb/ft^3	48.2	--	--
Water to cementitious ratio	--	0.38	0.46	0.46
High Range Water Reducing Admixture	ml	36	--	--
Target slump flow	in	24.0	30.25±0.25	34.0

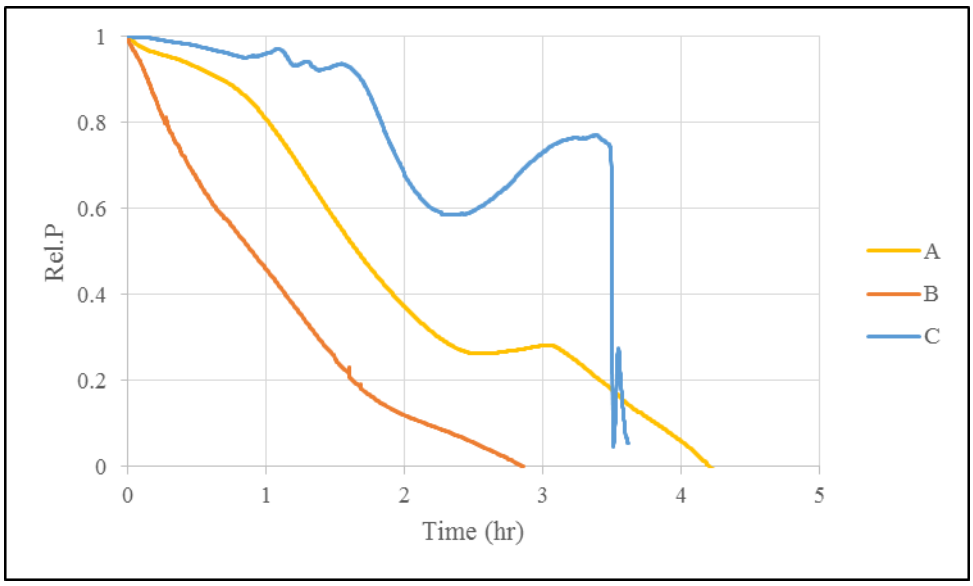

Figure 23 Relative formwork pressure (w.r.t max. hydrostatic pressure) variation with time measured using Form2

From the results in **Figure 23** for the mixes in **Table 11**, no comparison can be made about the rate of pressure decay as all the three mixes have different mix proportions and were cast on different days. However, by looking the pressure decay behavior, the last part of the curve is different for concrete, mortar and cement paste. The increase in the pressure (between 2 to 3 hours period) is more significant in cement paste, followed by mortar and then concrete indicating this difference is due to the aggregate. The mechanism for the increase in pressure is not known. Similar behavior was observed by Billberg [13] and by Lomboy et al. [33]. Lomboy et al. [33] attributed this behavior to the early expansion observed in the restrained shrinkage ring test for concrete as observed by the authors in Laomboy [34]. The reason for the expansion is not known may be it is related to the ettringite formation (Gauffinet [35]), but no study was done on cement paste to study the reason for this expansion.

Based on the results shown in **Figure 23**, expansion may be the reason for the increase because the concrete mix has the lowest increase in pressure. The aggregate may provide dimensional stability to the fresh concrete or mortar mix in formwork thereby partially making the mix support its weight thereby applying less lateral pressure on formwork.

The change in slope seen in the case of concrete before 2 hours was also observed by Khayat et al. [36]. The authors attributed the change in slope to change in the dominant mechanism causing the formwork pressure drop. Before the change in slope in **Figure 23**, the pressure drop was due to the physical phenomenon (reversible effect of thixotropy). The change in slope is because the chemical phenomenon (cement hydration) dominate the formwork pressure drop behavior.

4.1.4 Effect of addition of VMA

Effect of Viscosity Modifying Admixture (VMA) was studied by making two mixes (M1 and M2). Mix 1 (M1) was made without VMA. For Mix 2 (M2) all the proportions were kept same except for the addition of VMA. MasterMatrix VMA 362 was used in Mix2 as VMA. The mix proportions and the slump flow values for the mixes are shown in **Table 12**. Form2 was used for this study. Both mixes M1 and M2 were made on the same day (time difference of less than an hour) to make sure the environmental conditions (temperature and humidity) stay the same. The relative lateral pressure variation and yield stress gain over time data are shown in **Figure 24** and **Figure 25** respectively.

Table 12 Proportions of the evaluated mixtures

Materials	Units	M1	M2
Type I/II OPC	lb/ft^3	46.4	46.4
Water	lb/ft^3	18.5	18.5
Sand	lb/ft^3	72	72
Water to cementitious ratio	--	0.4	0.4
High Range Water Reducing Admixture	ml	70	70
Viscosity Modifying admixture	ml	--	100
Target slump flow	in	36.0±0.5	32.5±1.0

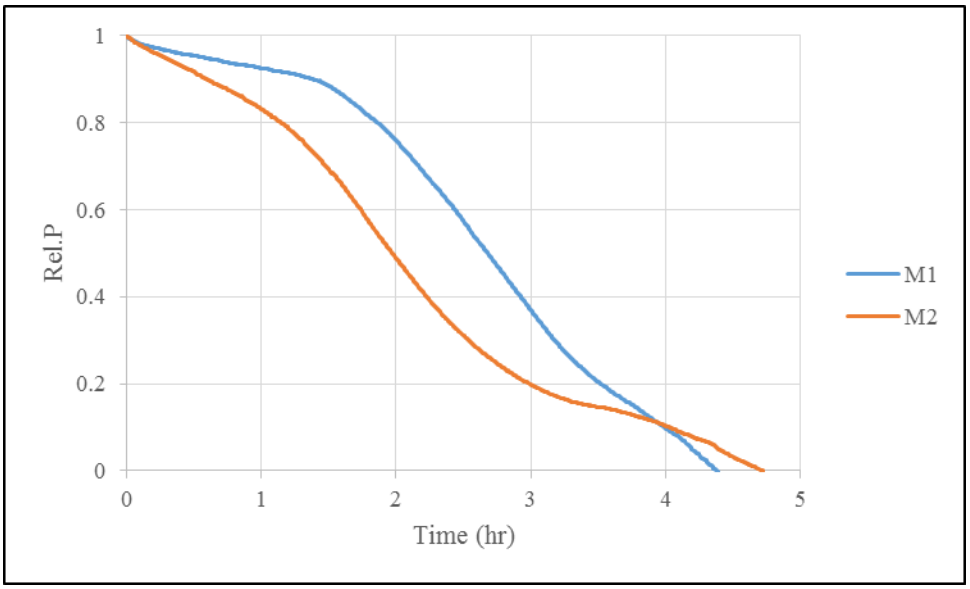

Figure 24 Relative formwork pressure (w.r.t max. hydrostatic pressure) variation with time for Form2

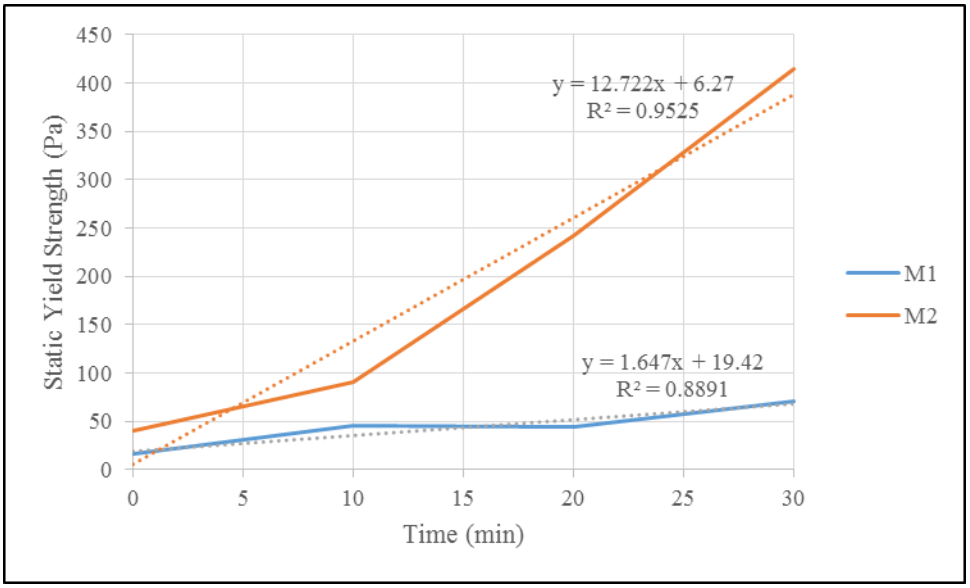

Figure 25 Static yield stress change over time for mixes M1 and M2

Figure 24 contains the relative pressure decay results for mixes M1 and M2. From the results, it is clear that the pressure decay is faster in the case of the mix with VMA (M2). From the static yield stress data in **Figure 25**, the yield stress gain is faster in mix M2 (based on the slope of the trendline equation). These results and from the literature review [section 0] implies that thixotropy starts to develop at a faster rate in the mix with VMA.

4.1.5 Effect of addition of fibers

Effect of fiber content on formwork pressure and static yield stress was studied by making three mixes (M1, M2, and M3). Mix 1 (M1) was made without any fibers, and for the other two mixes, fibers were added without changing any other proportions. Mix 3 (M3) contained double the amount fibers compared to Mix 2 (M2). STRUX 90/40 Synthetic Macro Fiber Reinforcement was used for mixes M2 and M3. The mix proportions and the slump flow values for the mixes are shown in **Table 13**. Form2 was used for this study. All the three mixes M1, M2, and M3, were made on the same day (with time difference of fewer than two hours) to make sure the

environmental conditions (temperature and humidity) stay the same. The relative lateral pressure variation and yield stress gain over time data are shown in **Figure 26** and **Figure 27** respectively.

Table 13 Proportions of the evaluated mixtures

Materials	Units	M1	M2	M3
Type I/II OPC	lb/ft^3	46.4	46.4	46.4
Water	lb/ft^3	18.5	18.5	18.5
Sand	lb/ft^3	72	72	72
Water to cementitious ratio	--	0.4	0.4	0.4
High Range Water Reducing Admixture	ml	70	70	70
Viscosity Modifying admixture	ml	100	100	100
Fibers	lb/ft^3		0.06	0.12
Target slump flow	in	32.5±1.0	32.0±0.5	33.0±1.0

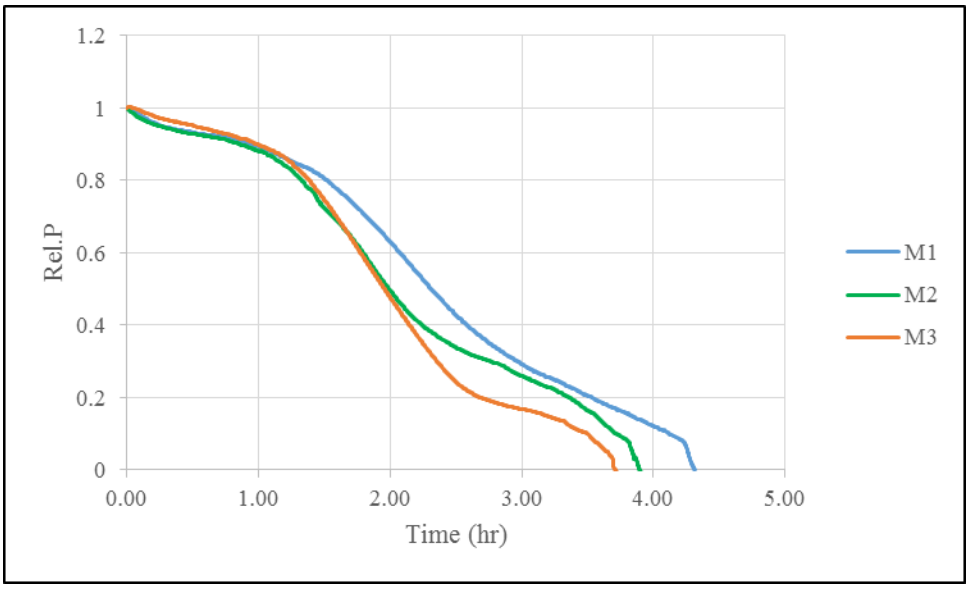

Figure 26 Relative formwork pressure (w.r.t max. hydrostatic pressure) variation with time for Form2

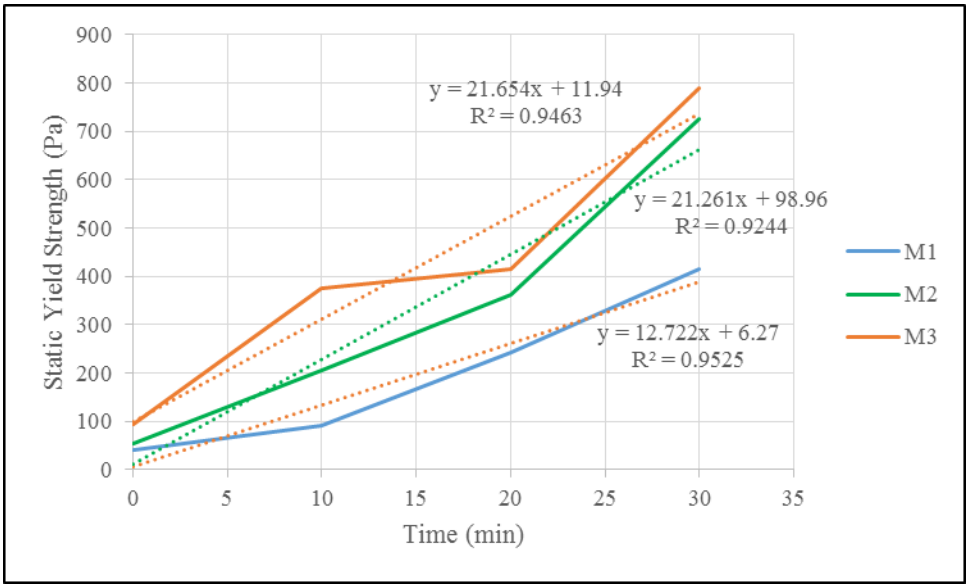

Figure 27 Static yield stress change over time for mixes M1, M2, and M3

Figure 26 contains the relative pressure decay results for mixes M1, M2, and M3. From the results, it is clear that the pressure decay is faster when the fibers are added, and also the decay seems to vary with the amount of fibers added. From the static yield stress data in **Figure 27**, the yield stress gain is faster for mix M3 (based on the slope of the trendline equation) compared to other two mixes. These results indicate that because of the presence of the fibers thixotropy starts to develop at a faster rate in mix M3.

4.2 Effect of Formwork Dimensions

The effect of formwork dimensions was studied by using formworks of varying dimensions. The schematic of the formwork used along with the dimensions and sensor locations are shown in **Figure 6** (copied in **Figure 28**). The sensors for Form1 and Form2 were attached at the height of 6in. from the base such that the effective height of concrete or mortar in the formworks were 30in. and 18in. respectively from the sensor. Similarly, for Form3, the sensors were attached at four different heights from the base (6in., 18in., 30in., and 42in.). This arrangement enabled to

understand the individual effect of length and diameter of the formwork on lateral pressure. Comparing between pressure decays for Form1 and Form2, the effect of different dimensions but same effective height (form height above the sensor) to diameter ratio was studied. Comparing the pressure decays between Form2 and Form3 (sensor at 1.5ft from top), the effect of the diameter was evaluated. Similarly comparing the pressure decays in Form3 for sensors located at 1.5ft and 4.5ft from the top, the effect of height was studied. The concrete (SCC1, SCC2, and SCC3), mortar (M1 and M2) and cement paste (C1) mix proportions used for this study are shown in **Table 14**. The formwork pressure decay collected for all the three formworks are shown in **Figure 29**, **Figure 30**, **Figure 31**, **Figure 32**, **Figure 33**, **Figure 34**, **Figure 35**, and **Figure 36**. The change in temperature with time in the formworks are shown in **Figure 37** and **Figure 38**.

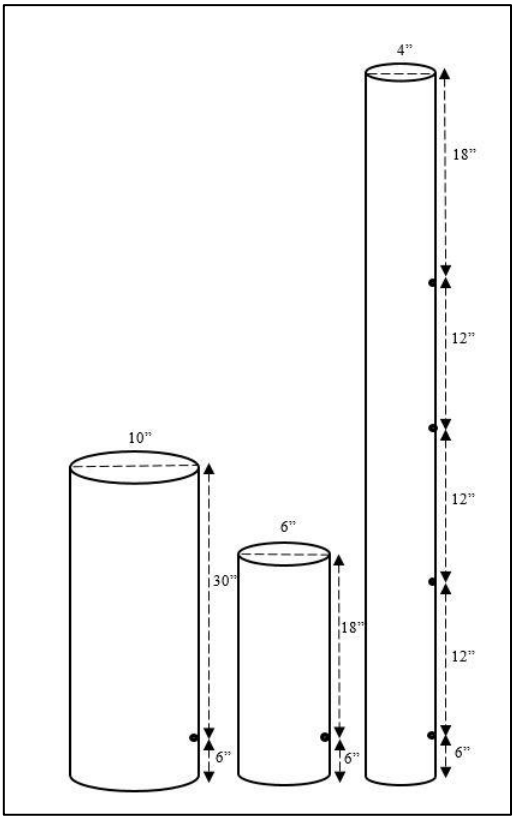

Figure 28 Schematic of the three formworks Form1, Form2, and Form3 (from left to right) along with the sensor location used

Table 14 Proportions of the evaluated mixtures

Materials	Units	SCC1	SCC2	SCC3	M1	M2	C1
Type I/II OPC	lb/ft^3	23.6	33.2	32.8	43.2	49.8	80.3
Class C Fly ash	lb/ft^3	7.2	--	--	--	--	--
Water	lb/ft^3	12.5	12.5	11.7	19.8	22.8	36.9
Sand	lb/ft^3	51.5	51.5	53.8	68.8	58.6	--
Limestone	lb/ft^3	48.2	48.2	48.7	--	--	--
Water to cementitious ratio	--	0.41	0.38	0.36	0.46	0.46	0.46
High Range Water Reducing admixture	ml	36	36	83	--	--	--
Viscosity Modifying Agent	ml	--	--	100	--	--	--
Target slump flow	in	28	24	28±0.5	33±0.5	37.5±1.5	34

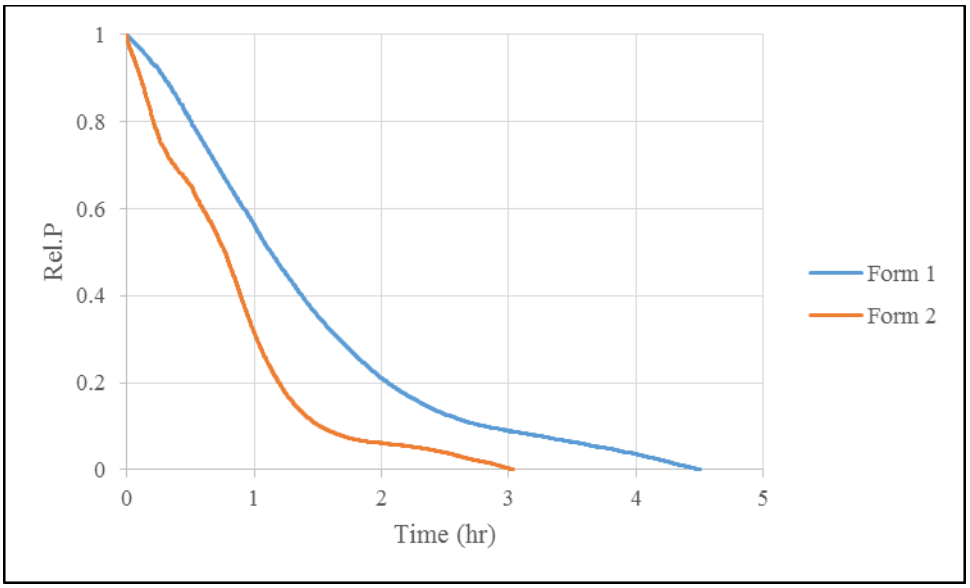

Figure 29 Relative formwork pressure (w.r.t max. hydrostatic pressure) variation with time for mix SCC1

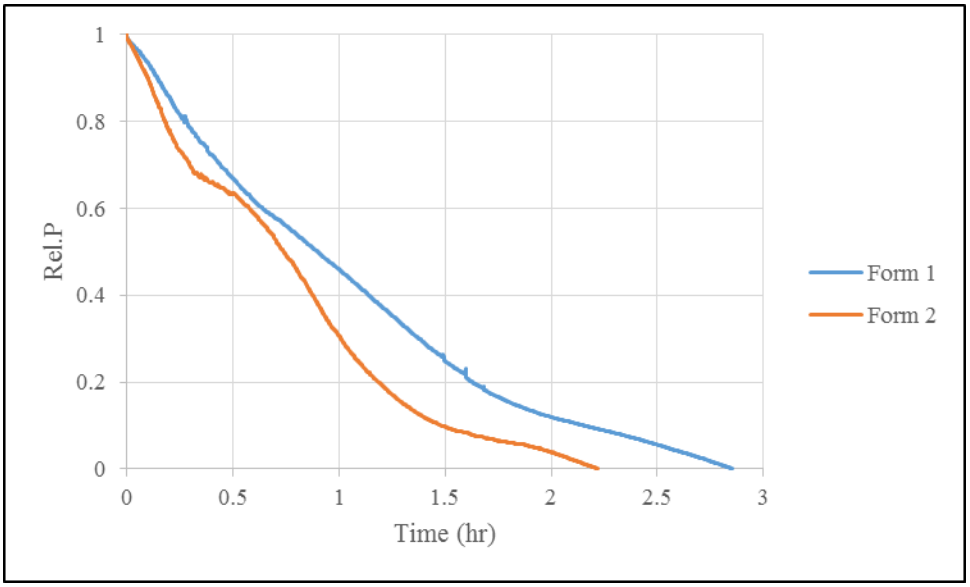

Figure 30 Relative formwork pressure (w.r.t max. hydrostatic pressure) variation with time for mix SCC2

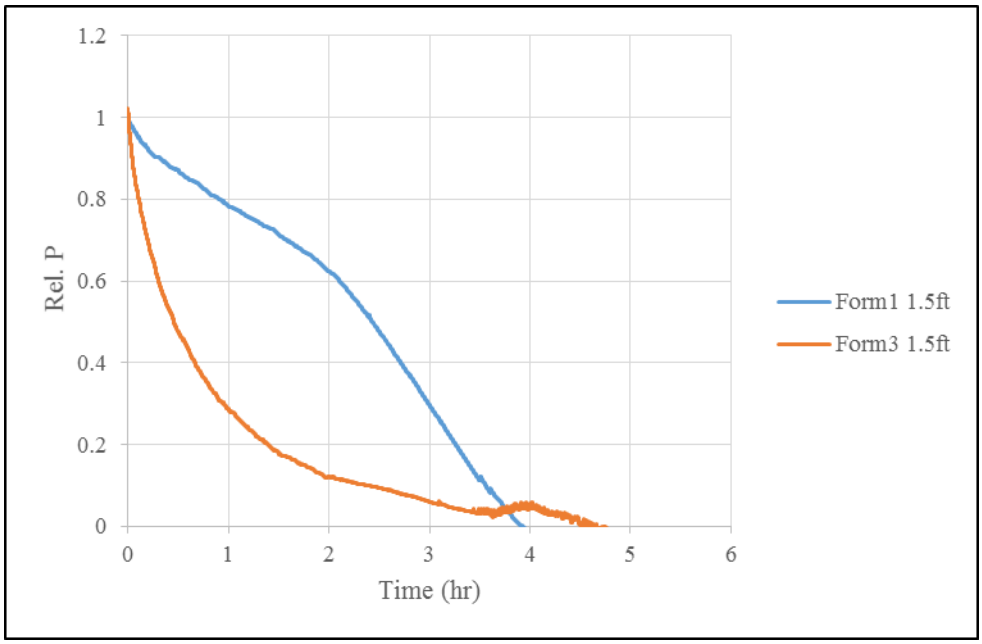

Figure 31 Relative formwork pressure (w.r.t max. hydrostatic pressure) variation with time for mix SCC3

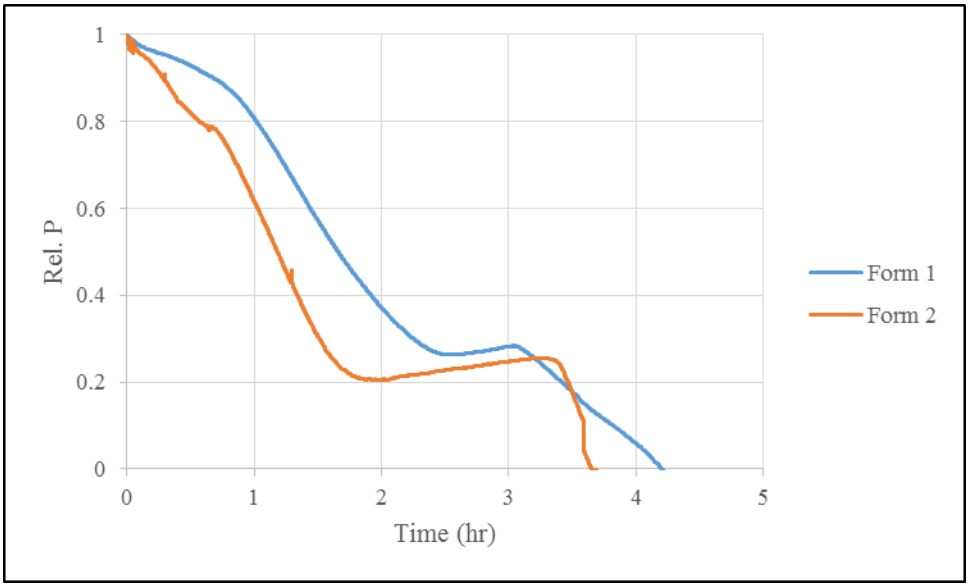

Figure 32 Relative formwork pressure (w.r.t max. hydrostatic pressure) variation with time for mix M1

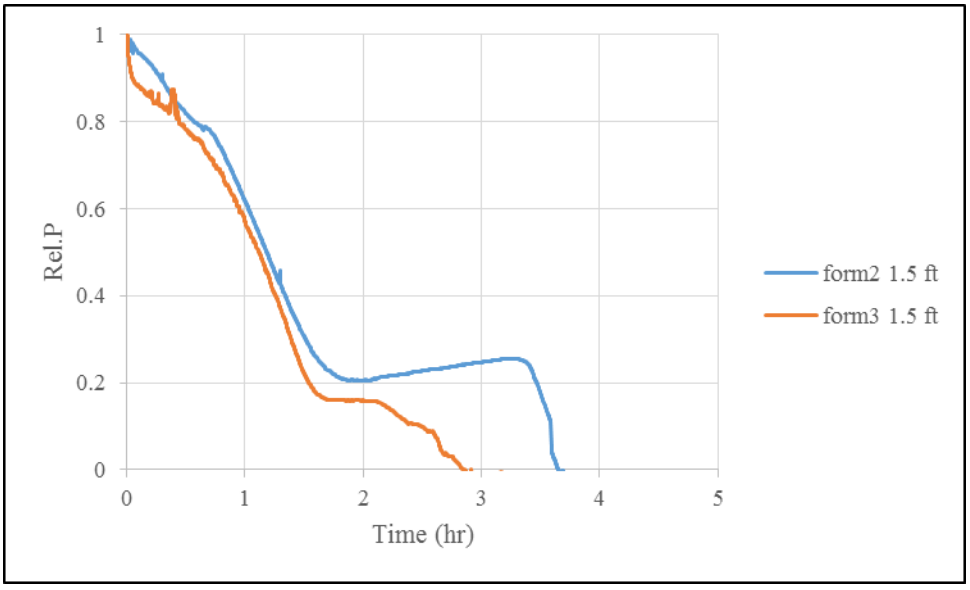

Figure 33 Relative formwork pressure (w.r.t max. hydrostatic pressure) variation with time for mix M1

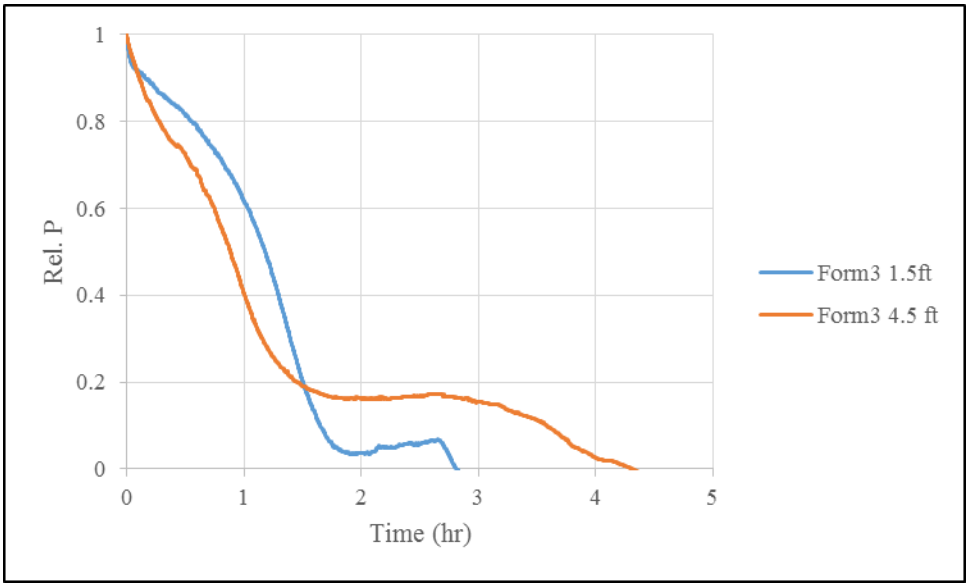

Figure 34 Relative formwork pressure (w.r.t max. hydrostatic pressure) variation with time for mix M1

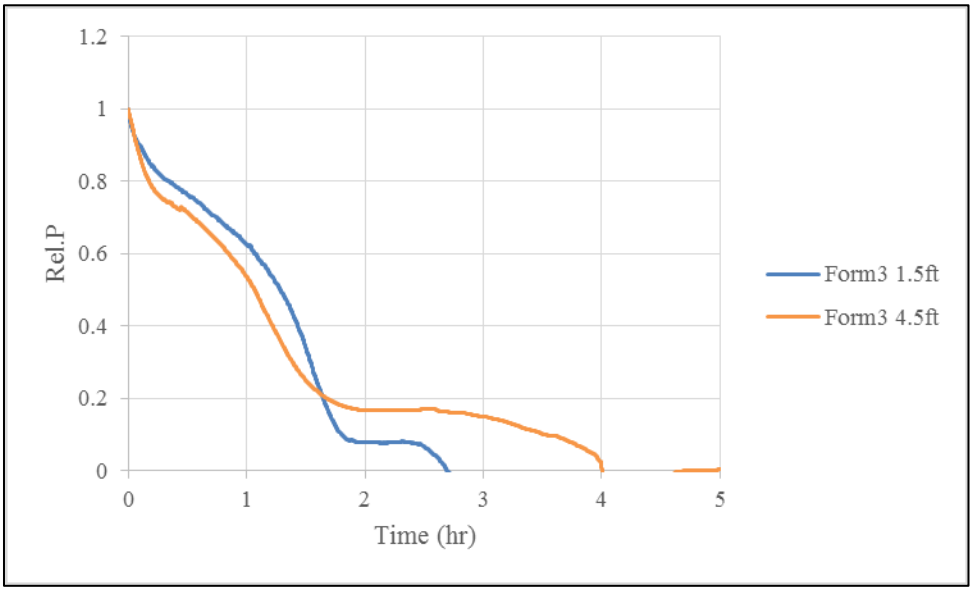

Figure 35 Relative formwork pressure (w.r.t max. hydrostatic pressure) variation with time for mix M2

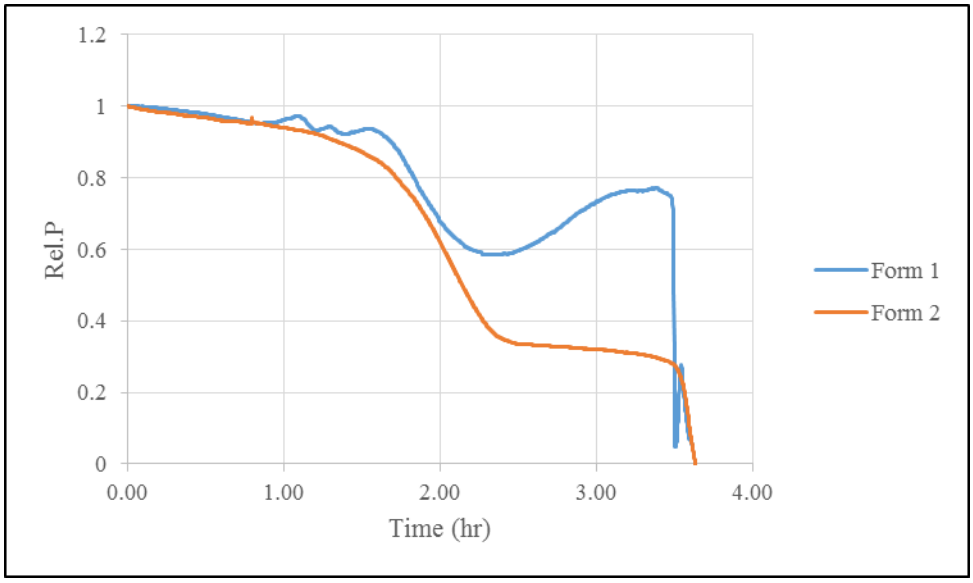

Figure 36 Relative formwork pressure (w.r.t max. hydrostatic pressure) variation with time for mix C1

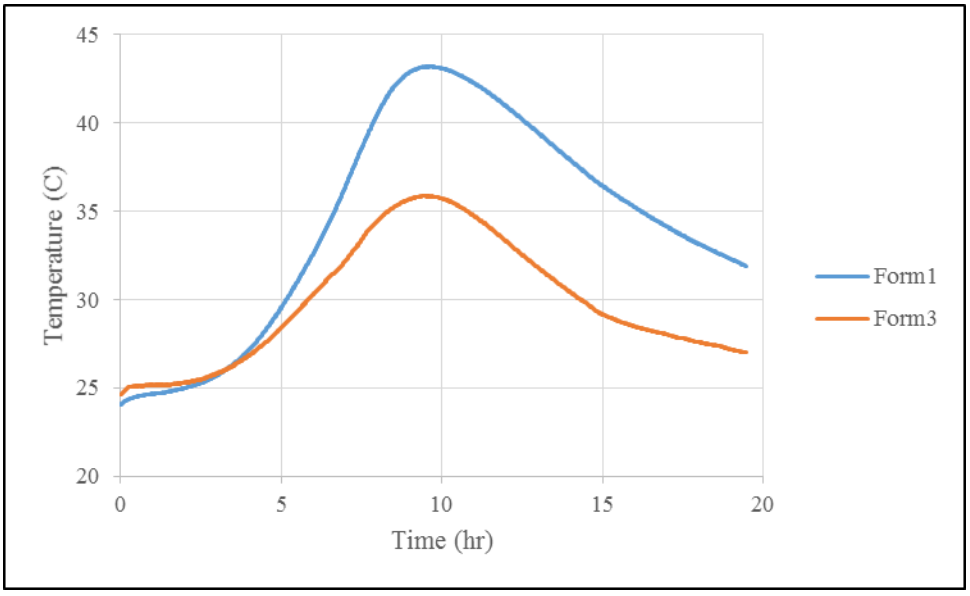

Figure 37 Temperature variation with time for mix SCC3 in formworks Form1 and Form3

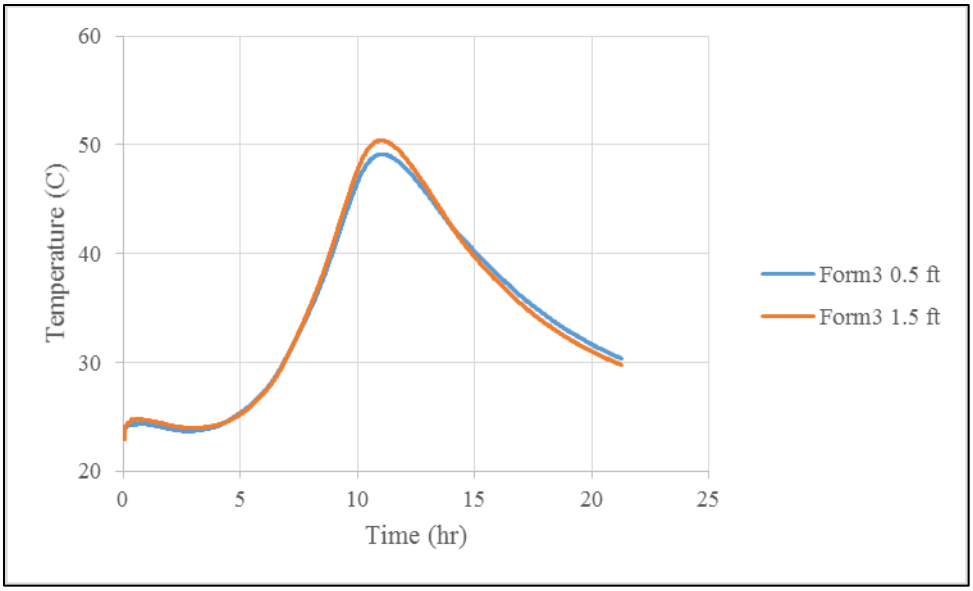

Figure 38 Temperature variation with time for mix C1 in Form3 at 0.5 ft and 1.5 ft depth

4.2.1 Same height and different diameter

Figure 31 is the formwork pressure decays for Form1, and Form3 with sensors at 1.5ft depth made using mix SCC3. **Figure 33** is the formwork pressure decays for Form2, and Form3 with sensors at 1.5ft made using mix M1. Based on the results, it is clear that the pressure decay is faster for the formwork with a smaller diameter. Theoretically, the pressure exerted should be independent of the cross section dimensions for a fixed depth. The initial lateral pressure is same for both formworks thereby giving same relative pressure value at zero hours (time at which the mortar was poured into the formwork and the formwork was manually disturbed to achieve the hydrostatic pressure value). However, as the time proceeds, the decay is faster in the narrower section. One of the reasons for this could be because in the narrower section surface area contact is higher between the concrete (or mortar) and formwork walls. So more lateral pressure is carried by the wall friction between the concrete (or mortar) and formwork. Also because of the smaller diameter in Form3 the concrete (or mortar) could not deform sufficiently to mobilize its full shearing resistance. This

phenomenon was called as an arching effect, and this phenomenon in the concrete formworks was explained by Rodin [9]. The difference in pressure decay between formworks is more predominant in the case of **Figure 31** compared to **Figure 33**. The reasons for that are the presence of coarse aggregate increases the arching action resulting in more decay in Form3 compared to Form1, and also the difference in the radius of the formwork is higher between Form3 and Form1 compared to Form3 and Form2.

In the narrower formwork, the aggregates are closer to each other. So there may be accelerated rate of stiffening of concrete due to the concentration of the pore solutions between the closely packed aggregate particles (this mechanism was suggested by Amziane et al. [11]).

The temperature data in forms Form1 and Form3 for mix SCC3 is shown in **Figure 37**. In Form1, due its bigger diameter and larger mass of concrete is filled into it compared to Form3. As a result higher temperature was observed in Form1. However, the temperature was significant after the first five hours, and in **Figure 31** the pressure decay is happening within the first five hours. So temperature may not be the reason for the pressure difference as suggested by Billberg [13] about the results observed by Khayat et al. [36]. In fact, in Khayat et al. [36], the authors observed that the decay is faster in the wider formwork which does not seem to be the case in the present study.

4.2.2 Same diameter and different height

Figure 34 and **Figure 35** are the formwork pressure decays for Form3 with sensors at 4.5 ft, and 1.5ft depth made using mixes M1 and M2 respectively. **Figure 38** has the temperature change for mix C1 and Form3 with sensors at different depths. Based on the results it is clear that the pressure decay is faster at deeper depths and there is no difference in temperature at different heights within a formwork. This may be due to the difference in the weight on the top of concrete or mortar as

the depth increases. Zhou et al. [37], Scherer et al. [38] observed that the presence of hydrostatic pressure has a significant effect on the kinetics of the dissolution of cement paste thereby affecting the rate of strength gain. Similar behavior was evident in the formwork results obtained in the work of Lomboy et al. [33]. It can also be observed that the pressure decay difference is smaller when the aggregate proportion is decreased.

4.2.3 Same height to diameter ratio

Figure 29 is the formwork pressure decays for Form1, and Form2 made using mix SCC1. Based on the results it is clear that the pressure decay is faster in Form2 compared to Form1. Similar results are observed for mix SCC2 shown in **Figure 30**. Comparing between SCC2 and SCC3 the concrete mixes are not very different (in terms of relative aggregate proportions). So from SCC3 mix data from **Figure 31**, it is clear that the pressure decay is vastly different in Form1 and Form2 when the sensors are located at the same depth. Increasing the depth from 1.5ft to 2.5ft the pressure would result in faster pressure decay and increasing the diameter from 6in to 10in result in slower pressure decay overall we see an increase in pressure decay in Form1 compared Form2. The difference in pressure drop seem to be again due to the presence of aggregate because from **Figure 36** which has the formwork pressure decays for Form1 and Form2 made using cement paste mix C1. The absence of aggregate in C1 resulted in same pressure decay in both forms independent of the difference in dimensions.

4.3 Effect of Thixotropy

Effect of thixotropy on pressure decay is observed by casting two identical pressure columns (using Form2 in **Figure 6**). One column is disturbed manually after every 10 minutes for approximately 30 seconds during first 50 minutes and then for every 20 minutes during the next

40 minutes. The other column was left undisturbed. Temperature changes within mortar pressure column were recorded using type T thermocouple and thermocouple data logger (USB TC-08). The temperature sensor was located at a depth of 1.5 feet from the top (0.5 feet from the bottom) of the formwork. Dynamic and static yield strength changes over time are recorded using ICAR rheometer to understand and differentiate between the reversible and irreversible changes in SCC after casting. The mortar mix used and its slump flow are shown in **Table 15**. Both the pressure columns used in this study were cast at the same time. A fresh batch of mortar mix was used for collecting each static yield stress data point. Moreover, the vane was inserted into the sample immediately after the mortar is poured into the ICAR container and left undisturbed until the static yield stress data is collected. For the dynamic yield stress data, the same sample was used for collecting all the data points as the dynamic yield stress does not depend on the shear history of the specimen. The pressure decay, yield strength data, and temperature data are shown in **Figure 39**, **Figure 40**, and **Figure 41** respectively.

Table 15 Proportions of the evaluated mixture

Materials	Units	M1
Type I/II OPC	lb/ft^3	46.4
Water	lb/ft^3	18.5
Sand	lb/ft^3	72.0
Water to cementitious ratio	--	0.40
High Range Water Reducing Admixture	ml	70
Viscosity Modifying admixture	ml	100
Target slump flow	in	35 ± 1.0

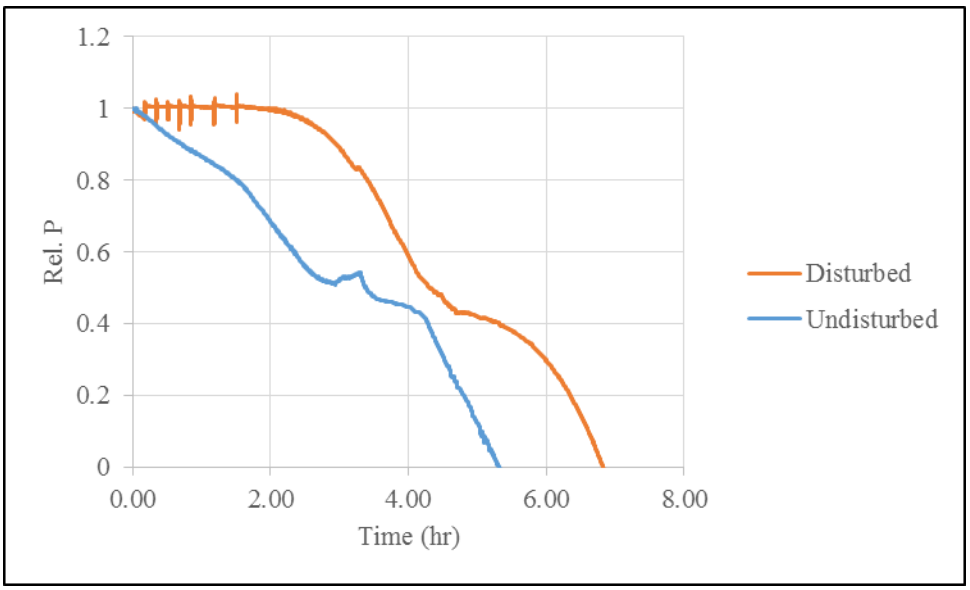

Figure 39 Relative formwork pressure (w.r.t max. hydrostatic pressure) variation with time for disturbed and undisturbed mixes

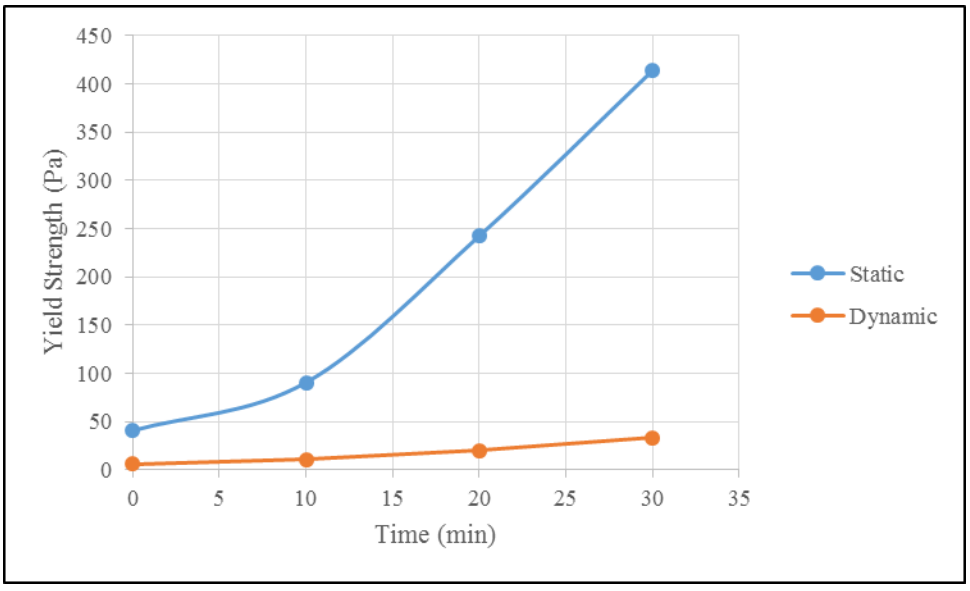

Figure 40 Static and dynamic yield strength change over time for mortar mix M1

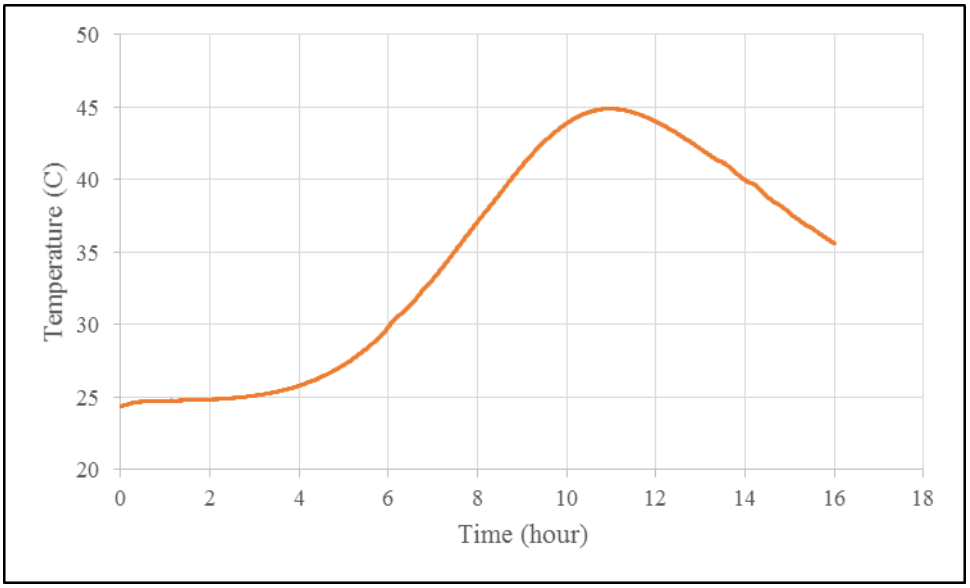

Figure 41 Temperature change over time in the undisturbed pressure column

In **Figure 39**, there is no pressure decay in the disturbed specimen within the first 2 hours, unlike the undisturbed specimen. From **Figure 40**, it can be observed that the static yield stress gain is much higher than the dynamic yield stress gain which means that the reversible mechanisms like flocculation dominate in the first 30 minutes tested. However, if the applied shear stress by the rheometer is not sufficient to break the reversible state (flocculation), then the dynamic yield stress values recorded not only account for the irreversible changes in the mortar but also the reversible changes that are not removed due to the limitation of the rheometer. A similar argument was made by Roussel [39], and the authors stated that none of the available rheometers have shear rate application capacity to break the material into the most deflocculated state (i.e., immediately after mixing) after a certain amount of resting period. This because the maximum shear rate they can apply to the material is always lower than the shear rate during mixing.

The temperature data was only reported in the undisturbed column in **Figure 41** because the temperature sensors in the other column failed to collect meaningful data. This is attributed to the intentional disturbance applied to the pressure column. However, from the reported temperature data, it can be observed that the temperature change started at around 4 hours indicating that there was no significant hydration happening before that (dormant period).

From the pressure decay data in **Figure 39**, it is clear that applying disturbance to the column lead to retain the fluid nature of mortar or in other words the maximum hydrostatic pressure as lateral pressure value in the first two hours. This indicates that the pressure drop in the undisturbed column at least in the first 2 hours is mainly due to thixotropy. The dynamic and static yield stress data and temperature data also supports the argument of the dominance of thixotropy in the initial stages of mortar after casting.

4.4 Rheology Test Methodology

The methodology for the measurement of static and dynamic yield stress values using ICAR rheometer is discussed in the experimental procedure section 0. For understanding the pressure decay, it is required to measure the change in yield stress values over time. The static yield stress value depends on the shear history of the test specimen. So if the same specimen is used for performing consecutive static yield stress measurements the specimen is slightly disturbed every time the peak torque is passed thereby producing inaccurate static yield stress values. In order to investigate this and to come up with a methodology for the accurate measurement of static yield stress, three mortar mixes (M1, M2, and M3) were studied. For each mix, two test setups were considered. In the first setup, the static yield stress values were collected consecutively over time in the same batch of mortar (i.e., the slightly disturbed specimen from previous reading is used for

the current reading). In the second setup, a fresh batch of mortar was used to collect yield stress data at each time (0 min, 10 min, 20 min, and 30 min). So for the first test setup, after mixing, the mortar was transferred into the ICAR container (within 9-10 min after addition of water to cement), and this was considered as 0 min. The vane was inserted into the mortar, and the static yield stress value was measured using the Stress growth test experimental procedure section 0. The test was stopped immediately after the torque reaches a peak value to minimize the disturbance within the material. The vane was left in the mortar, and the stress growth test was repeated after every 10 min. For the second test setup, fresh batch of mix (undisturbed) was used for collecting the data (i.e, for the data point collected at 10 min a different batch of mix (compared one used at 0 min) which was left undisturbed for 10 min (after mixing) in the ICAR container or the bucket is used). In the second test setup, the vane was inserted at different times for different mixes and is mentioned in detail in **Table 16** and the following paragraphs.

Mix 1 (M1) was made using ASTM C 150: "Standard Specification for Portland Cement" Type I Cement and water to cementitious ratio (w/cm) of 0.46 by weight. Mix 2 (M2) was also made using Type I Cement, but w/cm ratio was 0.38. Mix 3 (M3) was made using same proportions as M2 but cement used was Type I/II Cement. The mix proportions and the slump flow values for the mixes are shown in **Table 17**. ICAR rheometer and five-gallon buckets used for this study are shown in **Figure 42**. All the three mixes M1, M2, and M3, were made on the consecutive days, and the environmental conditions (temperature and humidity) more or less stayed the same during the testing period. The yield stress results are shown in **Figure 43**, **Figure 44**, and **Figure *45***.

Table 16 Test procedure adapted for each mix

Mix	Test Method
M1	Vane inserted into the mortar 3-4 min before the test
	Then Data collected continuously without taking the vane out from mortar
M2	Vane inserted into the mortar 3-4 min before the test
	Data collected by taking vane out after collecting each data point
M3	Vane is inserted into the mortar at 0 min
	Data collected continuously without taking the vane out from mortar

Table 17 Proportions of the evaluated mixtures

Materials	Units	M1	M2	M3
Cement*	lb/ft^3	43.2	45.7	45.7
Water	lb/ft^3	19.8	17.3	17.3
Sand	lb/ft^3	68.8	72.8	72.8
Water to cementitious ratio	--	0.46	0.38	0.38
Target slump flow	in	22± 0.5	17	18.25 ± 0.5

* M1 and M2 contained Type I cement, and M3 contained Type I/II cement

Figure 42 Rheology test setup used: 5 gallon bucket (left), ICAR container (right)

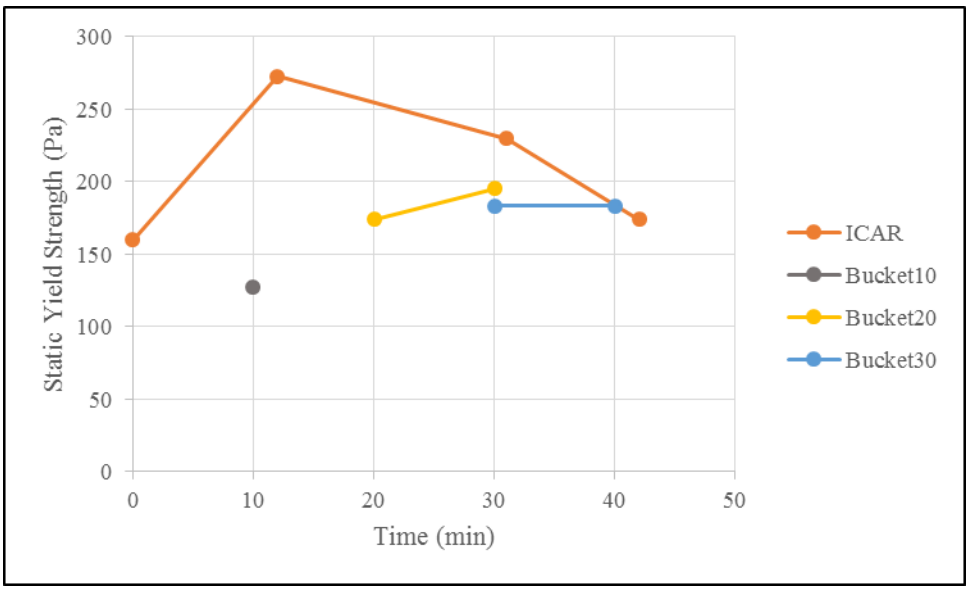

Figure 43 Static yield stress change over time for mix M1 measured using ICAR with mortar taken in ICAR container and Bucket

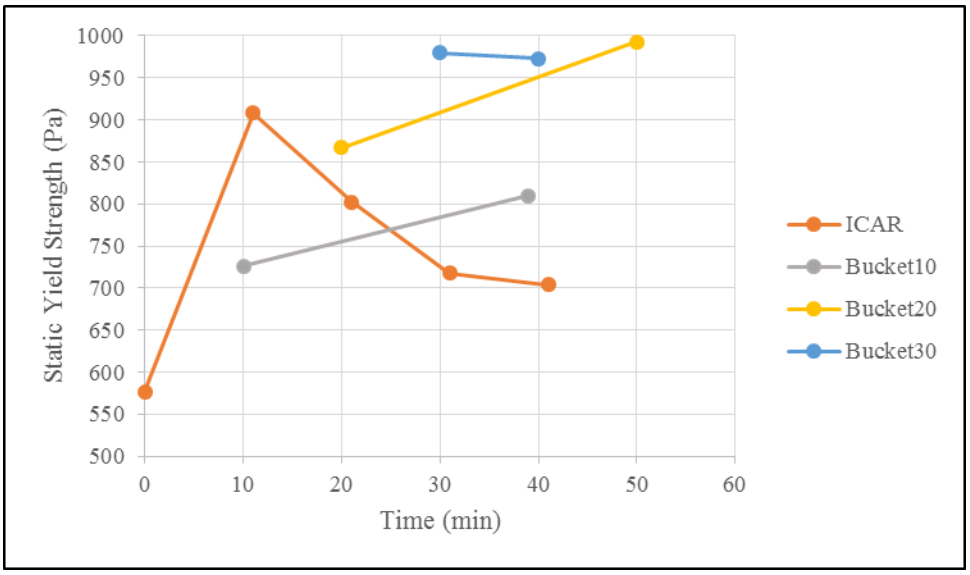

Figure 44 Static yield stress change over time for mix M2 measured using ICAR with mortar taken in ICAR container and Bucket

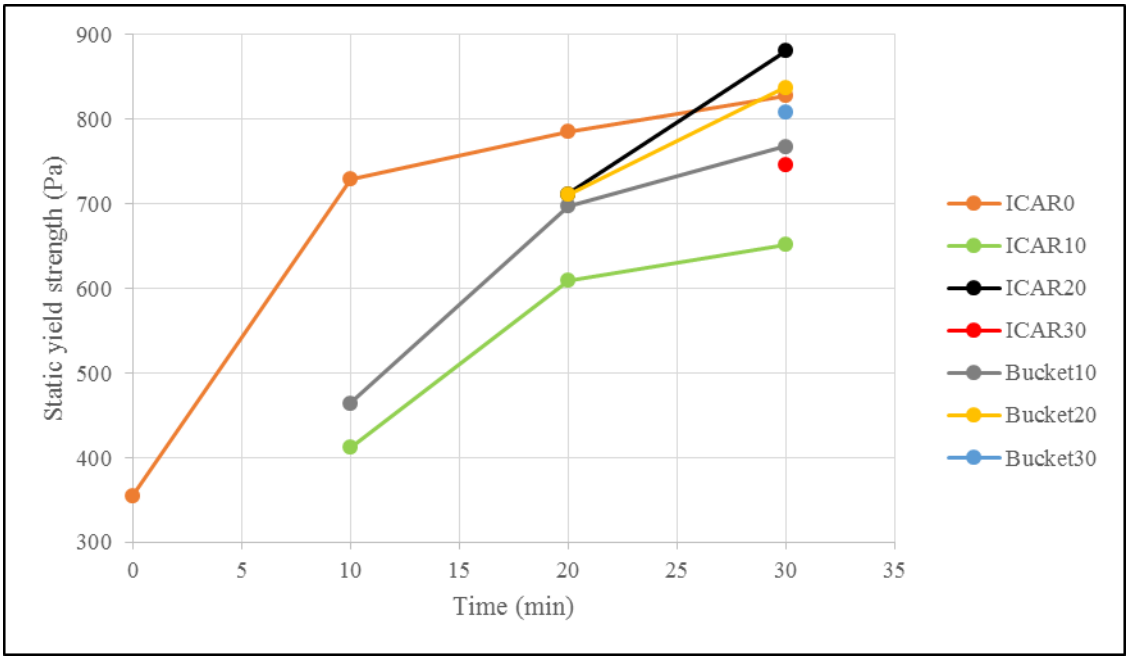

Figure 45 Static yield stress change over time for mix M3 measured using ICAR with mortar taken in ICAR container and Bucket

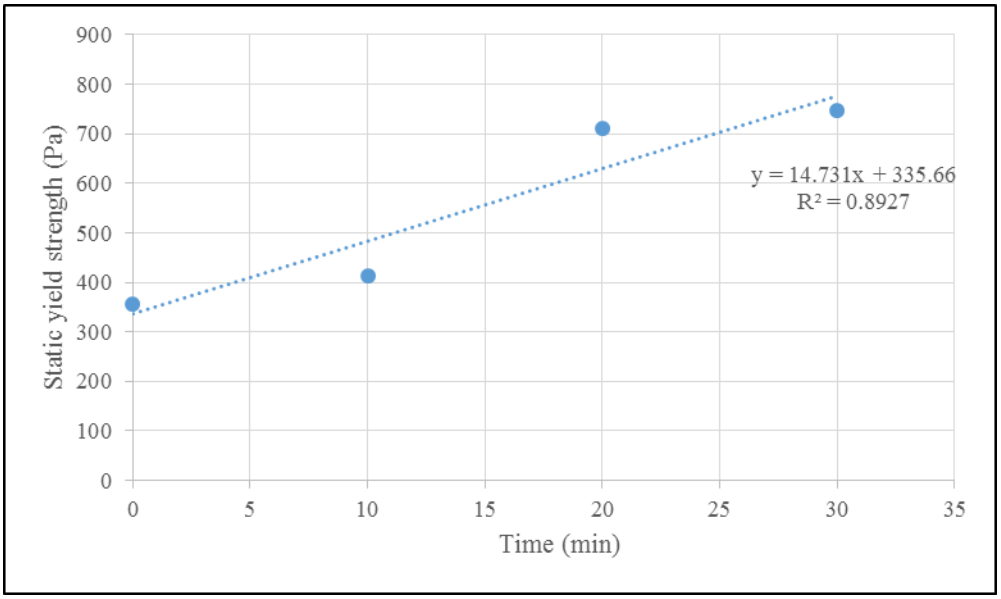

Figure 46 Static yield stress change over time for mix M3 measured using ICAR container and a new batch of mix for each test

In the above figures, the labels ICAR/Bucket indicates the container used and the number ICAR10/ICAR20 indicates the time the first stress growth test was conducted in that sample. Each batch of each mix was made to have more or less the same slump (with acceptable variation +/- 0.5 in from the reported values in **Table 17**).

Figure 43 is the static yield stress values over time for mix M1. As mentioned in **Table 16**, the vane is inserted into each batch of the mix at time 3 to 4 minutes before the stress growth test. For the data labeled as ICAR in **Figure 43**, the vane is in the mortar at 0 min, and the stress growth test was conducted immediately. After the toque reached a peak value the test was stopped. The vane was left in the mortar, and the test was conducted after10, 20, and 30 minutes. However, for data labeled as Bucket20, the vane was inserted in the undisturbed mix 3 to 4 minutes before the test, i.e., around 16 to 17 minutes after the mortar was poured into the bucket and after the test the vane was left in a mortar and the test was conducted again after 10 minutes. Similar procedure was adopted for Bucket10 and Bucket30.

Figure 44 is the static yield stress values over time for mix M2. In that figure, for data labeled ICAR similar procedure was adopted as for mix M1. However, for Bucket10, after collecting data at 10 minutes, the vane was taken out of the sample and reinserted 3 to 4 minutes before the next test, i.e., after 16 to 17 minutes to get the data at 30 minutes. Similar procedure was adopted for data for Bucket20 and Bucket30.

Figure 45 is the static yield stress values over time for mix M3. For Mix M3, the vane was inserted into each batch of the mix at time 0 minutes, i.e., immediately after mixing and pouring the mix into the ICAR container or bucket. For each stress growth test, the test was stopped immediately after the peak torque is reached to avoid further disturbance and this was done to minimize the disturbance to mortar as much as possible.

From the above figures, comparing the data for ICAR label, the static yield stress data is decreasing over time for mixes M1 and M2. That is because the stress growth test was not stopped immediately after reaching the peak torque thereby disturbing the sample. Based on the results for mix M3 it is clear that however much the disturbance is minimized the static yield stress values should not be taken in the specimen that is disturbed. The ICAR container used has dimensions of 12 inch dimete,r and 12.3 inch length and the buckets used have dimensions of 12 inch diameter at the top, 10.3 inch diameter at the bottom and 14.5 inch length. The dimensions of the bucket and the ICAR container are different. This explains the difference in static yield stress values for mix M3 using ICAR container and buckets in **Figure 45**. However, no correlation can be established between the dimensions of the container used and yield stress values. The static yield stress more or less seems to vary linearly as per Mix M3 data in **Figure 46**. A similar observation has been by Billberg [13], Ovarlez et al. [26]. Based on the results for all the mixes M1, M2, and M3, it is clear that when the mix is disturbed slightly the yield stress value obtained is higher than the stress value obtained in a fresh batch of mortar. Contrary, i.e., disturbance lead to an underestimation of the structural build-up is expected. Similar observation was made by Billberg [13]. This strain hardening behavior is also observed by Min et al. [40]. The authors observed that the cement paste showed strain hardening response at high strain levels under squeeze flow at the same time the authors attributed such behavior partly to the geometry of the specimen. Based on the results obtained, it is clear that same batch of material should not be used for measuring the static yield stress change over time. So a new batch of mortar/ concrete is used for the static yield stress value documented in this report.

4.5 Effect of using different pressure sensors and Sensor Calibration

The reliability of the pressure data acquired from the sensors was checked, and the accuracy was improved by adding two sensors on the formwork at the same height as shown in **Figure 47**. The black dots in **Figure 47** indicates the sensor location. The average of values from the two sensors was reported as the formwork pressure for the experiments conducted using From1 and Form2 in this report. For the data using Form3, only one sensor was used at each height to record the lateral pressure.

The calibration of the sensors was done by checking the resistance across the ends of the Wheatstone bridge when the bridge is balanced. The pressure values were also checked, and the scaling factors (ratio of the actual pressure value to the value measured by the pressure sensor) were adjusted by conducting formwork lateral pressure experiments with water. The formwork made of same material and thickness of Form3 but with diameter 4 inches and height 24 inches was used for the study. The sensors were attached at a depth of 18 inches from the top. The water was poured into the formwork. From the height of the water above the sensor, the hydrostatic pressure value was computed. This value was compared with the pressure value measured by the sensor, and the scaling factors were computed. The temperature sensitivity of the sensors was checked by pouring the hot water (temperature around 50^0C) into the formwork, and the temperature and pressure data were collected over time. The pressure and temperature data are shown in **Figure 48** and **Figure 49** respectively. The results shown are for the two different pressure sensors used. One of the pressure sensors had a pressure range of 0 to 100 psi (sensor 1), and another one had a range 0 to 15 psi (sensor 2).

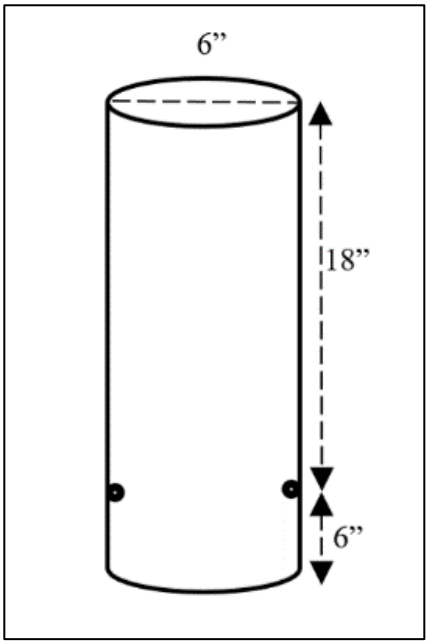

Figure 47 Schematic of the form along with the sensor location with dimensions in inches

To avoid any damage to the sensors, a thin plastic film was placed between the sensor diaphragm and the concrete. To check that if the film was interfering with the pressure measured by the sensor, the pressure data was collected by using two sensors (one with film and other without) that were installed on the same formwork at the same height. The mortar was poured into the formwork and the pressure decay data over time was recorded. The pressure and temperature results from this test are shown in **Figure 50** and **Figure 51**.

For low pressure range sensors (pressure range 0 to 15 psi), aggregate impingement on the diaphragm caused resulted in the damage of the sensors as shown in **Figure 52**. As a result, a sponge as shown in **Figure 52** along with the thin film was used between the sensor and concrete to prevent the damage. The data collected for concrete mix with and without sponge are shown in **Figure 53** and **Figure 54**.

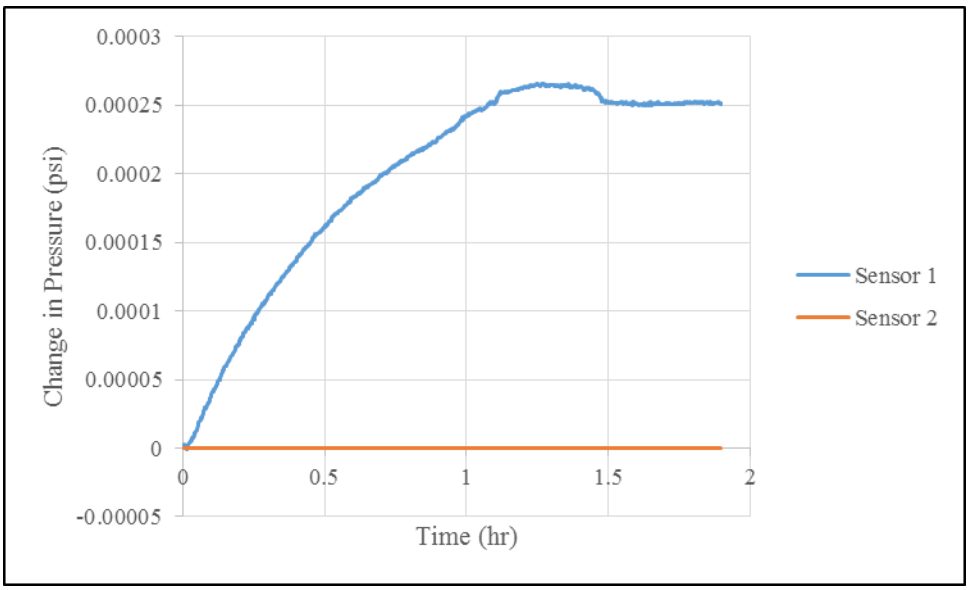

Figure 48 Change in lateral pressure with time for water

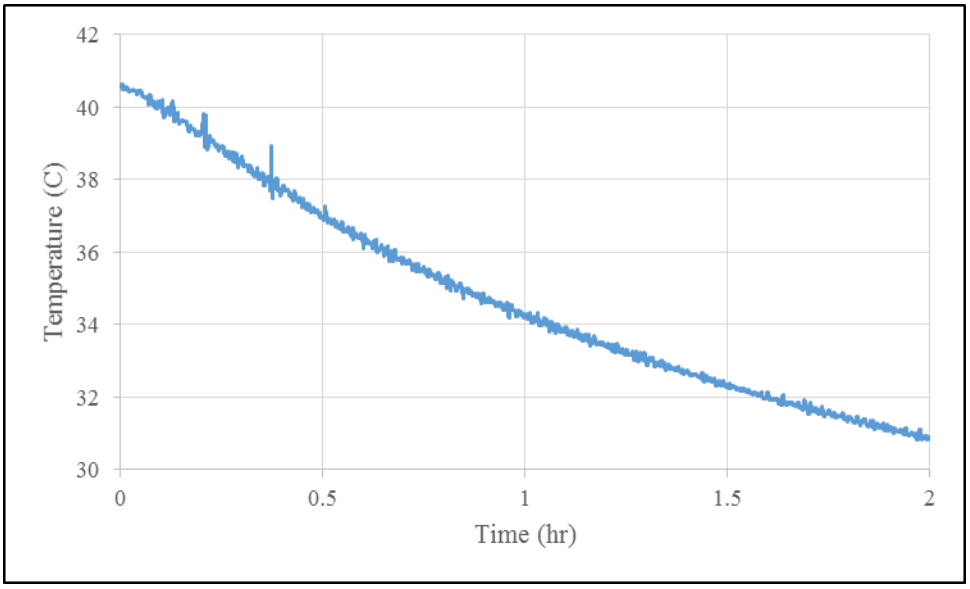

Figure 49 Change in temperature of water in formwork with time

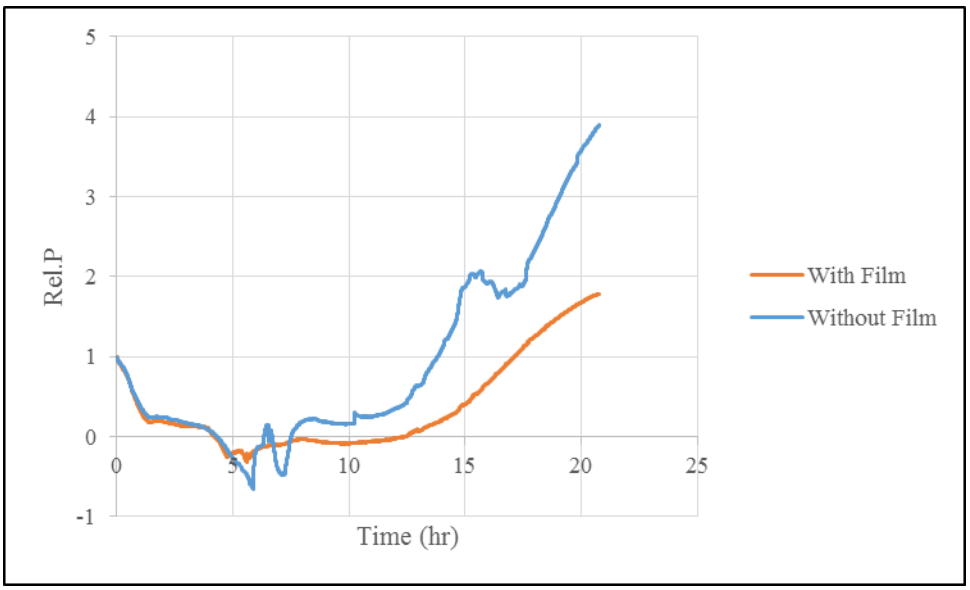

Figure 50 Relative formwork pressure (w.r.t max. hydrostatic pressure) variation with time

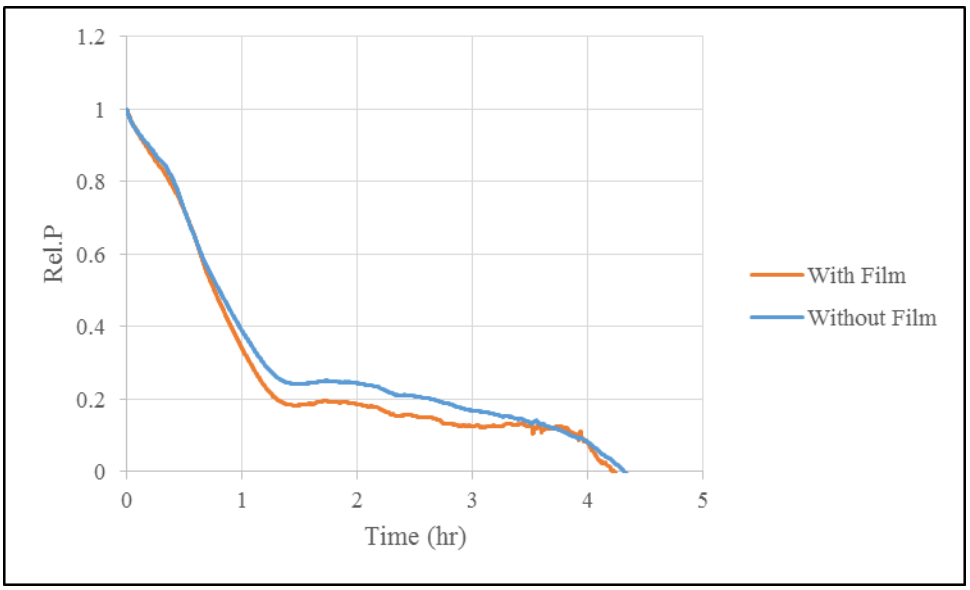

Figure 51 Relative formwork pressure (w.r.t max. hydrostatic pressure) variation with time before the pressure drops below zero

Figure 52 Damage of the sensor (left) due to impingement of the aggregates and sponge added (right)

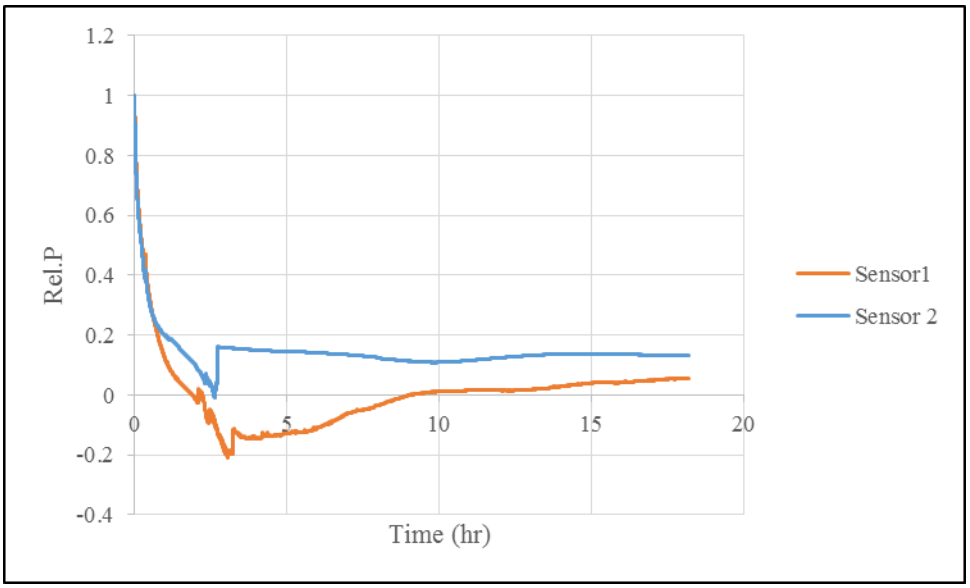

Figure 53 Relative formwork pressure (w.r.t max. hydrostatic pressure) variation with time

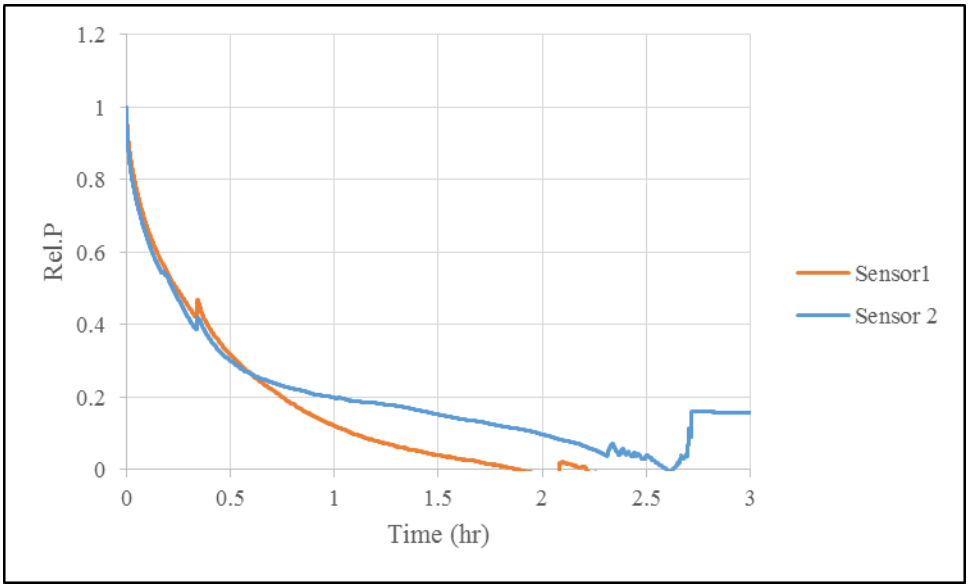

Figure 54 Relative formwork pressure (w.r.t max. hydrostatic pressure) variation with time before the pressure drops below zero

In **Figure 48**, the change in the pressure values over time for the hot water poured into formwork is shown. The corresponding change in temperature of the water is shown in **Figure 49**. The temperature of the water was raised up to 50^0C to simulate the high temperature in concrete due to hydration process. From the pressure change results, it can be confidently said that the pressure sensor data acquired by the sensor is accurate even when the temperature of the concrete raises over time. The pressure data presented in this work is before the temperature increase due to hydration. So it can be concluded that the sensors provided accurate data without any error due to temperature changes.

In **Figure 50** and **Figure 51**, the change in the pressure values over time for the mortar with two sensors of the same pressure range (0 to100 psi) are shown. For the two sensors, one of them had a film attached between the concrete and sensor, and another one did not. **Figure 51** shows the pressure data for both the sensors in the first few hours before the pressure drops to zero. From

Figure 51, it can be observed that adding the film does not affect the initial pressure decay (in first 30 to 45 minutes) and beyond that, the sensor without any film shows the slightly higher value of relative pressure. From **Figure 50**, beyond the five-hour mark, the pressure drops below zero and then increases again. The reason for this increase in pressure may be due to the expansion of mortar as observed in the restrained shrinkage ring test in Lamboy et al. [34]. Billberg [13] also observed the similar behavior of increase in pressure, but the author attributed this behavior the way the test was setup. The pressure test setup used by the author consist of a stainless steel tube with each end sealed with bolted plates and an air valve attached to the top plate to simulate high concrete pressures (condition of taller formwork). The author suggested that the overpressure might increases the tube diameter and/or when the concrete gets stiff enough it contracts to result in the overpressured air getting in between the concrete and the tube wall ultimately leading to increase in the pressure recorded by the pressure cell. In our present study, there is no overpressure applied on the formwork so the explanation provided by Billberg [13] may not be completely accurate.

The drop in pressure below zero may be due to the shrinkage and using the film seemed to have reduced the amount of shrinkage and expansion recorded by the sensor. This shrinkage behavior was also considered by Billberg [13] to explain the change in formwork pressure decay behavior after a few hours of casting. For all the pressure decay measurements done in this work, plastic film was used along with the sensors as it does not seem to effect the pressure data significantly at least in the pressure decay region this work focusses on.

In **Figure 53** and **Figure 54**, the change in the pressure values over time for the mortar with two sensors with different pressure ranges (sensor 1: 0 to 100 psi and sensor 2: 0 to 15 psi) are shown. A sponge material was added to the diaphragm of sensor 2 to prevent any aggregate impingement. **Figure 54** shows the pressure data for both the sensors in the first few hours before the pressure

drops to zero. From **Figure 54**, it can be observed that adding the film does not affect the initial pressure decay (in the first 30minutes) and beyond that, the sensor 2 with sponge shows the slightly higher value of relative pressure. From **Figure 53**, the pressure does not drop below zero for sensor 2 with sponge indicating that because of the presence of sponge and the plastic film the shrinkage experienced by concrete is not transferred or recorded by the sensor. The reason for the increase in pressure after 2.5 hours is partially explained in the previous paragraphs. For all the pressure decay measurements done in this work using sensor 2, plastic film and sponge were used as it does not seem to effect the pressure data significantly at least in the pressure decay region this work focusses on.

4.6 Predicting pressure decay using the Lange and Tejeda model

The pressure decay data obtained using different concrete mixes and formworks in the above sections was used to predict the lateral pressure exerted by SCC on a wall of 40 feet tall for a filling rate 8ft/hr. Lange and Tejeda model (explained in section 0) was used for predicting the pressure. The objective of this analysis was to evaluate the effectiveness of Lange and Tejeda model in predicting formwork pressure. The pressure data collected from different formwork sizes is used for this study. The details of the SCC mixes used shown in **Table 18** and **Table 19**. The measured and modeled pressure decay curves are shown in **Figure 55**, **Figure 56**, **Figure 57**, **Figure 58**, **Figure 59**, **Figure 60**, **Figure 61**, and **Figure 62**.

Table 18 Proportions of the evaluated mixtures

Materials	Units	SCC1	SCC2	SCC3	
Type I/II OPC	lb/ft^3	33.2	23.6	32.8	
Class C Fly ash	lb/ft^3	--	7.2	--	
Water	lb/ft^3	12.5	12.5	53.8	
Sand	lb/ft^3	51.5	51.5	48.7	
Limestone	lb/ft^3	48.2	48.2	11.7	
Water to cementitious ratio	--	0.38	0.41	0.36	
High Range Water Reducing Admixture	ml	36	36	83.0	
Viscosity Modifying Agent	ml	--	--	100.0	
				Mix A	**Mix B**
Target slump flow	in	24	28	27	28.5

Table 19 Particle size distribution of the coarse aggregate

Mix	A	B
Sieve Size	**% Retained on each sieve**	
0.75 in	0.0	5.0
0.5 in	0.0	40.0
0.375 in	5.0	42.5
No.4	57.5	7.5
No.16	37.5	5.0

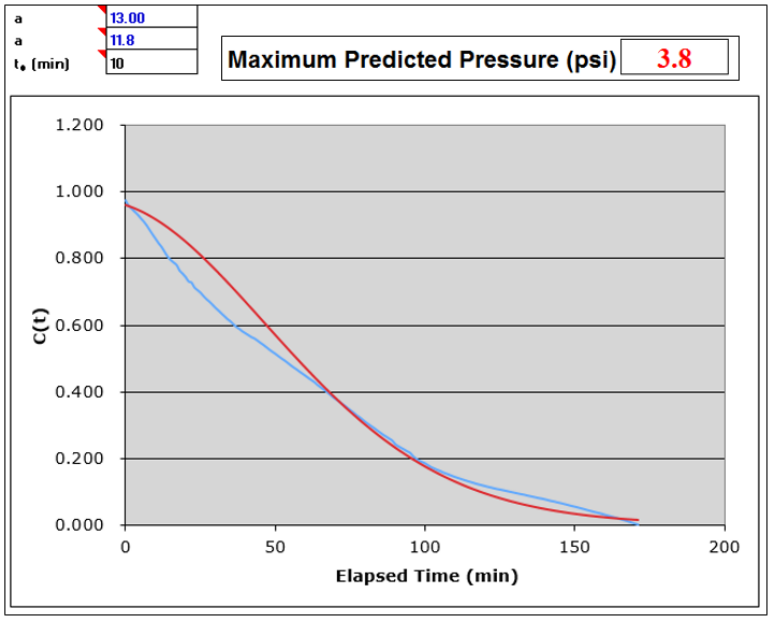

Figure 55 Measured and modeled pressure decay values for SCC1 using Form1

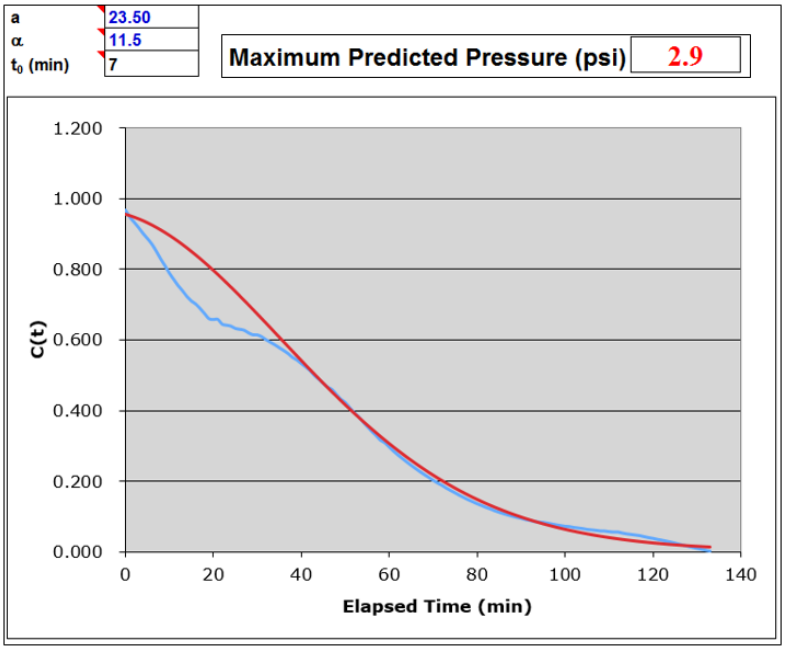

Figure 56 Measured and modeled pressure decay values for SCC1 using Form2

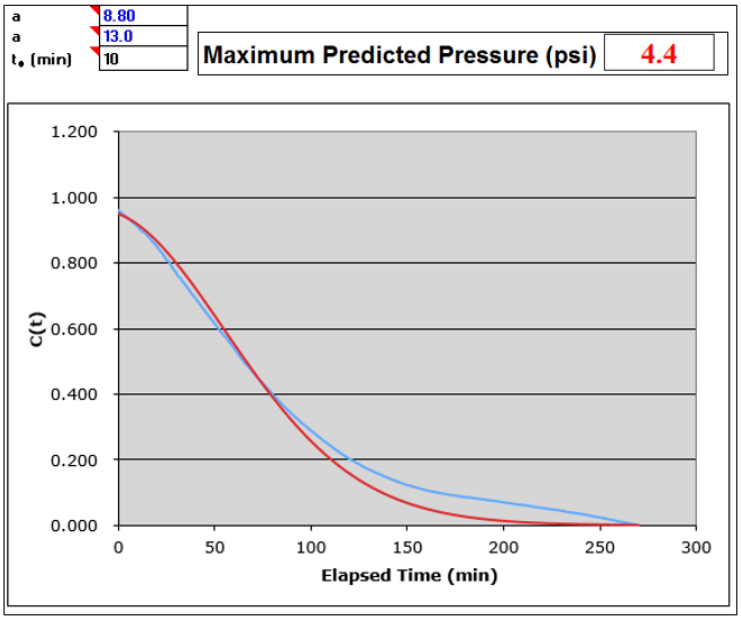

Figure 57 Measured and modeled pressure decay values for SCC2 using Form1

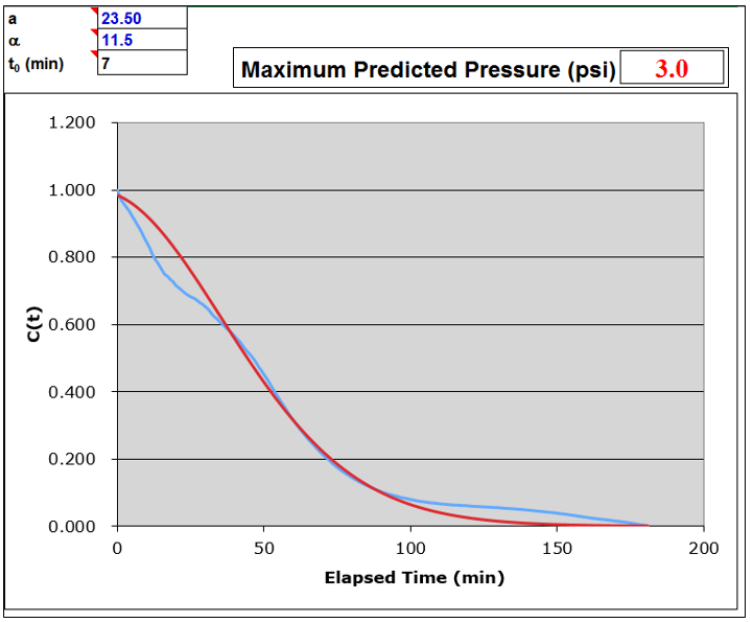

Figure 58 Measured and modeled pressure decay values for SCC2 using Form2

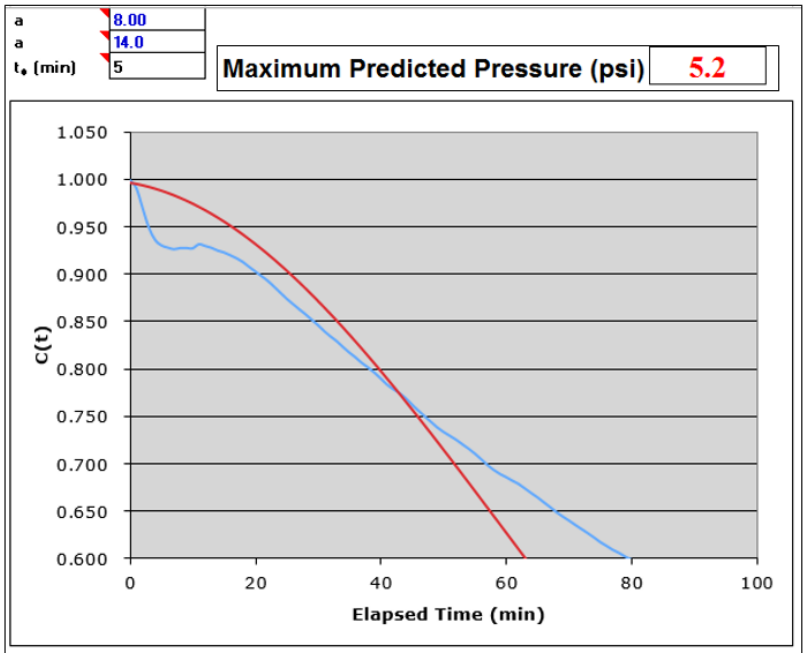

Figure 59 Measured and modeled pressure decay values for SCC3A using Form1

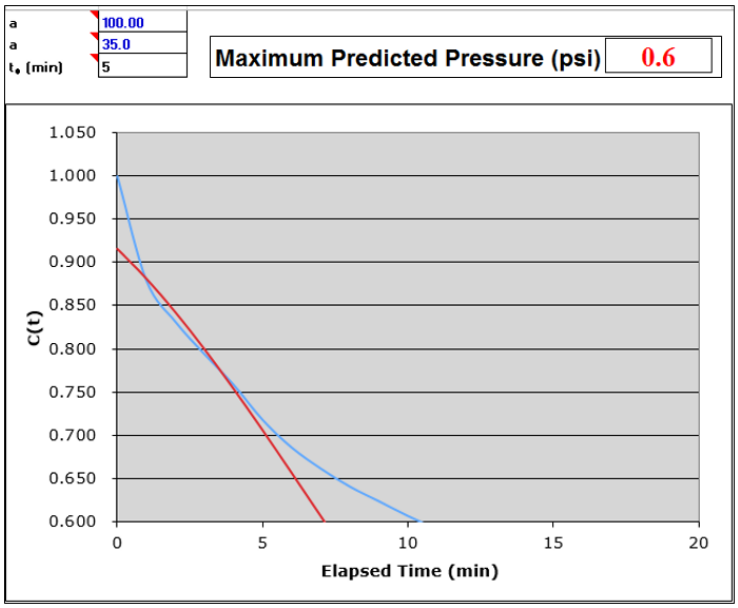

Figure 60 Measured and modeled pressure decay values for SCC3A using Form3

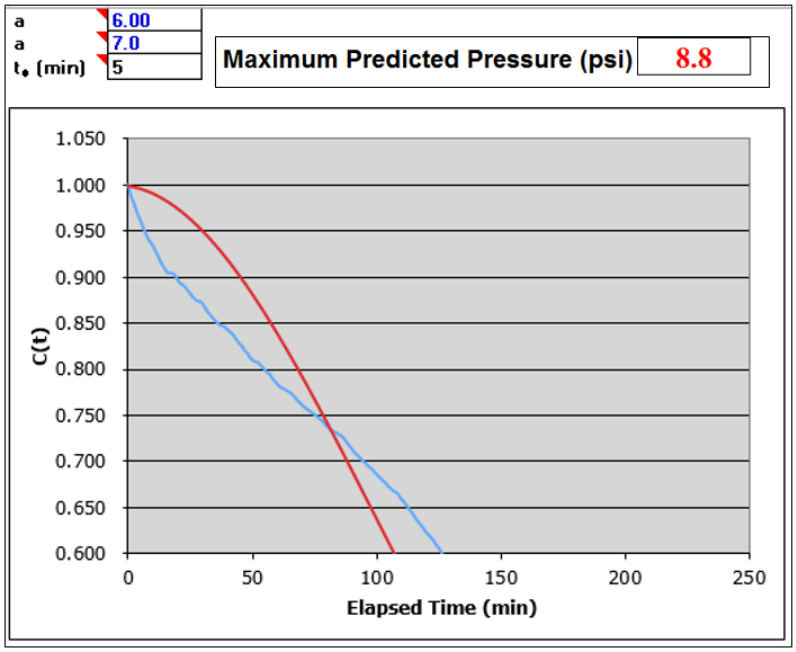

Figure 61 Measured and modeled pressure decay values for SCC3B using Form1

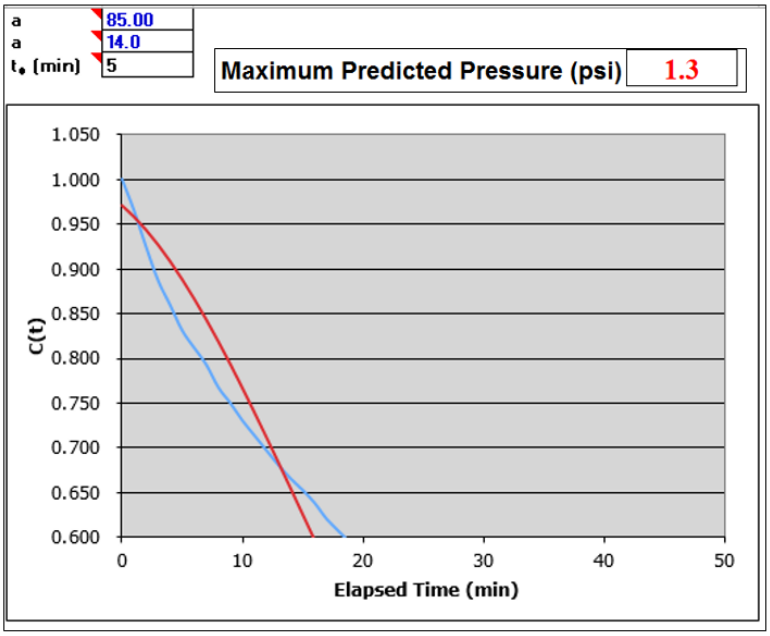

Figure 62 Measured and modeled pressure decay values for SCC3B using Form3

Table 20 Predicted maximum pressure for the mixes for 40ft. wall

Concrete Mix	Formwork (diameter (in.))	Predicted max. pressure (psi)
SCC1	Form1 (10 in.)	3.8
	Form2 (6 in.)	2.9
SCC2	Form1 (10 in.)	4.4
	Form2 (6 in.)	3.0
SCC3A	Form1 (10 in.)	5.2
	Form3 (4 in.)	0.6
SCC3B	Form1 (10 in.)	8.8
	Form3 (4 in.)	1.3

The predicted pressure value should be same for a given concrete mix independent of the size of the formwork used. However, from **Table 20** the predicted pressure values are different when different formwork sizes are used. The difference in pressure values is more significant when the difference in formwork dimensions is higher. The reason for the lower value of predicted maximum pressure for smaller formwork is explained in section 0. These results indicate the

importance of formwork dimensions in predicting pressure decay. So a correction factor that accounts for formwork dimensions needs to be included in the Lange and Tejeda model for the accurate prediction of the lateral pressure.

CHAPTER 5

CONCLUSIONS AND RECOMMENDATIONS

Throughout the course of this work, various concrete, mortar, and cement paste mixes were evaluated to understand the formwork pressure decay. Mix design parameters like the water to cement ratio, aggregate properties (size, moisture content, and quantity), admixtures (mineral and chemical), and fiber content and formwork dimensions were varied. Based on the experimental formwork pressure data and rheology data the following conclusions and recommendations are made.

5.1 Conclusions

5.1.1 Mix Design Parameters

Decreasing the water to cementitious ratio (w/cm) results in less fluid mix and faster pressure decay. High range water reducing admixture influences the effects w/cm ratio has on pressure decay behavior.

Replacement of cement with class C fly ash by volume results in a mix with more workability, lower yield stress, lower yield stress gain over time, and slower pressure decay. However, the effect depends on the composition and size of fly ash particles.

The absorption of the moisture by the aggregates when submerged in water to achieve SSD does not happen within 24 hours as specified in ASTM C127 – 15: “Standard Test Method for Relative Density (Specific Gravity) and Absorption of Coarse Aggregate.” The moisture content of the aggregates has a significant affect the pressure decay.

The presence of aggregate or increasing the amount of aggregate in mortar or concrete mix results in faster pressure decay and gain in static yield stress. The presence of aggregate also suppresses the increase in pressure after the pressure decay in first few hours. The increase in pressure after the decay in first few hours is attributed to the expansion of cement paste and the reasons for the expansions is not known.

The maximum aggregate size influences the pressure decay. The effect of aggregate size on formwork pressure decay also depends on the dimensions of the formwork used. However, for a given formwork dimension, the smaller the aggregate size faster is pressure decay.

The addition of VMA and/or fibers increases the static yield strength gain of self consolidating mortar/concrete. As a result, the pressure decay is faster when VMA and/or fibers are added.

5.1.2 Formwork dimensions and Rheology

Formwork dimensions have a significant effect on the pressure decay. Pressure decay varies due to the change in both diameter and height of the formwork. The effect of form diameter on pressure decay also depends on the aggregate size. However, for a given aggregate size and proportion, decrease in the diameter of the formwork results faster decay due to arching effect and increase in the lateral pressure carried by the wall friction between the concrete and formwork.

Even when the casting is fast, without any time for static yield stress development, the pressure decay is faster as the depth of the formwork increases, and the decay also varies with the aggregate content. This behavior is attributed to the increase in the reaction kinetics in the cement paste due to the weight of concrete as the depth increases. When the height to diameter ratio is kept constant, the pressure decay seems to decrease for form with smaller diameter and height indicating that the effect of diameter is more significant for the dimensions considered in this test.

The yield strength gain is due to reversible and irreversible changes in concrete/mortar. However, in the first few hours, the reversible changes dominate. The study of dynamic, static yield strength and temperature changes help to differentiate between the reversible and irreversible structural changes in concrete causing the pressure decay.

Self consolidating mortars exhibit strain hardening behavior, i.e., the yield stress value for disturbed mortar is higher than the stress value obtained in a fresh batch of mortar. For measuring the static yield stress or the thixotropy of SCC, a new sample needs to be used for each test measurement. The shear history influences the static yield stress data significantly.

5.2 Recommendations

Based on information collected from the literature review and the experimental program, some of the recommendations are made to improve the methods for measuring and modelling the formwork pressure for SCC. From the mix design point of view, using the oven dried aggregates (with fines sieved off) and aggregate with low absorption capacity is recommended as it offers better control over the mix in terms of available water in the concrete mix for workability and hydration thereby controlling the variation formwork pressure. Effect of water range admixtures in terms of its dosage and its type on pressure decay was not explored in the present study and it needs to be explored because based on the literature review and the experimental data, it is evident that the effect of the mineral and other chemical admixtures not only depend on their properties but also on their interaction with water reducing admixtures. The formwork dimensions (height, diameter, and height to diameter ratio) have a significant on the pressure decay so its effect should be considered when developing the models for the estimation of formwork pressure. Reversible effects dominate the pressure decay for the first few hours so to understand the pressure decay

completely the fresh properties of concrete and cement paste with emphasis on the thixotropy and its behavior under constrained and creep load conditions need to be studied. A small variation in the material proportions affect the pressure decay, yield stress data significantly making the prediction of the field lateral pressure exerted by a concrete mix based on the results obtained in the laboratory studies.

CHAPTER 6

REFERENCES

1. Okamura, Hajime, and Masahiro Ouchi. "Self-compacting concrete." *Journal of advanced concrete technology* 1.1 (2003): 5-15.
2. ACI, I. "347-Guide to Formwork for Concrete." *American Concrete Institute International* (2004).
3. Khayat, K. H., and A. F. Omran. "State-of-the-art review of form pressure exerted by self-consolidating concrete." *Final Report Ready-Mix Concrete (RMC) Research and Education Foundation, American Concrete Institute (ACI), and Strategic Development Council (SDC)* (2009).
4. Gardner, N. J. "Pressure of concrete on formwork-A review." *Journal Proceedings*. Vol. 82. No. 5. 1985.
5. Felekoğlu, Burak, et al. "The effect of fly ash and limestone fillers on the viscosity and compressive strength of self-compacting repair mortars." *Cement and concrete research* 36.9 (2006): 1719-1726.
6. Assaad, Joseph. *Formwork pressure of self-consolidating concrete influence of thixotropy*. Université de Sherbrooke, 2004.
7. Khayat, Kamal H. "Viscosity-enhancing admixtures for cement-based materials—an overview." *Cement and Concrete Composites* 20.2-3 (1998): 171-188.
8. Ghio, Virgilio A., Paulo JM Monteiro, and Laura A. Demsetz. "The rheology of fresh cement paste containing polysaccharide gums." *Cement and concrete research* 24.2 (1994): 243-249.

9. Rodin, Stanley. "PRESSURE OF CONCRETE ON FORMWORK." *Proceedings of the Institution of Civil Engineers* 1.6 (1952): 709-746.
10. Omran, A. F., K. H. Khayat, and Y. M. Elaguab. "Effect of SCC mixture composition on thixotropy and formwork pressure." *Journal of Materials in Civil Engineering* 24.7 (2011): 876-888.
11. Amziane, S., and Ph Baudeau. "Effects of aggregate concentration and size in fresh concrete pressure on formwork walls." *Materials and Structures* 33.1 (2000): 50-58.
12. Assaad, Joseph, and Kamal H. Khayat. "Effect of coarse aggregate characteristics on lateral pressure exerted by self-consolidating concrete." *ACI Materials Journal* 102.3 (2005): 145.
13. Billberg, Peter. Form pressure generated by self-compacting concrete: influence of thixotropy and structural behaviour at rest. Diss. Byggvetenskap, 2006.
14. Roby, H. G. "Pressure of concrete on forms." *Civil Engineering* 5.3 (1935).
15. Bensted, John. "Early hydration of Portland cement—effects of water/cement ratio." *Cement and Concrete Research* 13.4 (1983): 493-498.
16. Khayat, Kamal H., and Joseph J. Assaad. "Effect of w/cm and high-range water-reducing admixture on formwork pressure and thixotropy of self-consolidating concrete." *ACI Materials Journal* 103.3 (2006): 186.
17. Omran, Ahmed F., and Kamal H. Khayat. "Effect of Formwork Characteristics on SCC Lateral Pressure." *Journal of Materials in Civil Engineering* (2016): 04016293.
18. Leemann, Andreas, Cathleen Hoffmann, and Frank Winnefeld. "Pressure of self-consolidating concrete on formwork." *Concrete International* 28.02 (2006): 28-31.

19. Tejeda-Dominguez, Fernando. *Laboratory and Field Study of Self-Consolidating Concrete (SCC) Formwork Pressure*. 2005.
20. Perrot, A., et al. "SCC formwork pressure: influence of steel rebars." *Cement and Concrete Research* 39.6 (2009): 524-528.
21. Arslan, Metin, Osman Şimşek, and Serkan Subaşı. "Effects of formwork surface materials on concrete lateral pressure." *Construction and Building Materials* 19.4 (2005): 319-325.
22. Santilli, A., I. Puente, and M. Tanco. "A factorial design study to determine the significant parameters of fresh concrete lateral pressure and initial rate of pressure decay." *Construction and Building Materials* 25.4 (2011): 1946-1955.
23. Gardner, N. J., et al. "Field investigation of formwork pressures using self-consolidating concrete." *Concrete international* 34.1 (2012): 41-47.
24. Clear, C. A., and T. A. Harrison. *Concrete pressure on formwork*. CIRIA, 1985.
25. Khayat, Kamal H., and Ahmed F. Omran. "Field validation of SCC formwork pressure prediction models." *Concrete international* 33.6 (2011): 33-39.
26. Ovarlez, G., and N. Roussel. "A physical model for the prediction of lateral stress exerted by self-compacting concrete on formwork." *Materials and Structures* 39.2 (2006): 269-279.
27. Graubner, Carl-Alexander, et al. "Formwork pressure induced by highly flowable concretes–design approach and transfer into practice." *Structural Concrete* 13.1 (2012): 51-60.
28. Vanhove, Y., C. Djelal, and A. Magnin. "Prediction of the lateral pressure exerted by self-compacting concrete on formwork." *Magazine of concrete research* 56.1 (2004): 55-62.

29. Billberg, Peter H., et al. "Field validation of models for predicting lateral form pressure exerted by SCC." *Cement and Concrete Composites* 54 (2014): 70-79.
30. Janssen, H. A. "Versuche über getreidedruck in silozellen." *Zeitschr. d. Vereines deutscher Ingenieure* 39.35 (1895): 1045-1049.
31. Roussel, Nicolas, ed. *Understanding the rheology of concrete*. Elsevier, 2011.
32. Alhozaimy, Abdulrahman M. "Effect of absorption of limestone aggregates on strength and slump loss of concrete." *Cement and Concrete Composites* 31.7 (2009): 470-473.
33. Lomboy, Gilson R., Xuhao Wang, and Kejin Wang. "Rheological behavior and formwork pressure of SCC, SFSCC, and NC mixtures." *Cement and Concrete Composites* 54 (2014): 110-116.
34. Lomboy, Gilson, Kejin Wang, and Chengsheng Ouyang. "Shrinkage and fracture properties of semiflowable self-consolidating concrete." *Journal of Materials in Civil Engineering* 23.11 (2010): 1514-1524.
35. Gauffinet-Garrault, S. "The rheology of cement during setting." Understanding the Rheology of Concrete (2011): 96.
36. Khayat, Kamal, et al. "Effect of section width and casting rate on variations of formwork pressure of self-consolidating concrete." *Materials and structures* 38.1 (2005): 73-78.
37. Zhou, Qizhi, and James J. Beaudoin. "Effect of applied hydrostatic stress on the hydration of Portland cement and C3S." *Advances in Cement Research* 15.1 (2003): 9-16.
38. Scherer, George W., Gary P. Funkhouser, and Sulapha Peethamparan. "Effect of pressure on early hydration of class H and white cement." *Cement and Concrete Research* 40.6 (2010): 845-850.

39. Roussel, Nicolas. "A thixotropy model for fresh fluid concretes: theory, validation and applications." *Cement and Concrete Research* 36.10 (2006): 1797-1806.
40. Min, B. H., L. Erwin, and H. M. Jennings. "Rheological behaviour of fresh cement paste as measured by squeeze flow." *Journal of materials science* 29.5 (1994): 1374-1381.

APPENDIX A

LABVIEW CODE

A.1 LabVIEW code for pressure data acquisition using NI

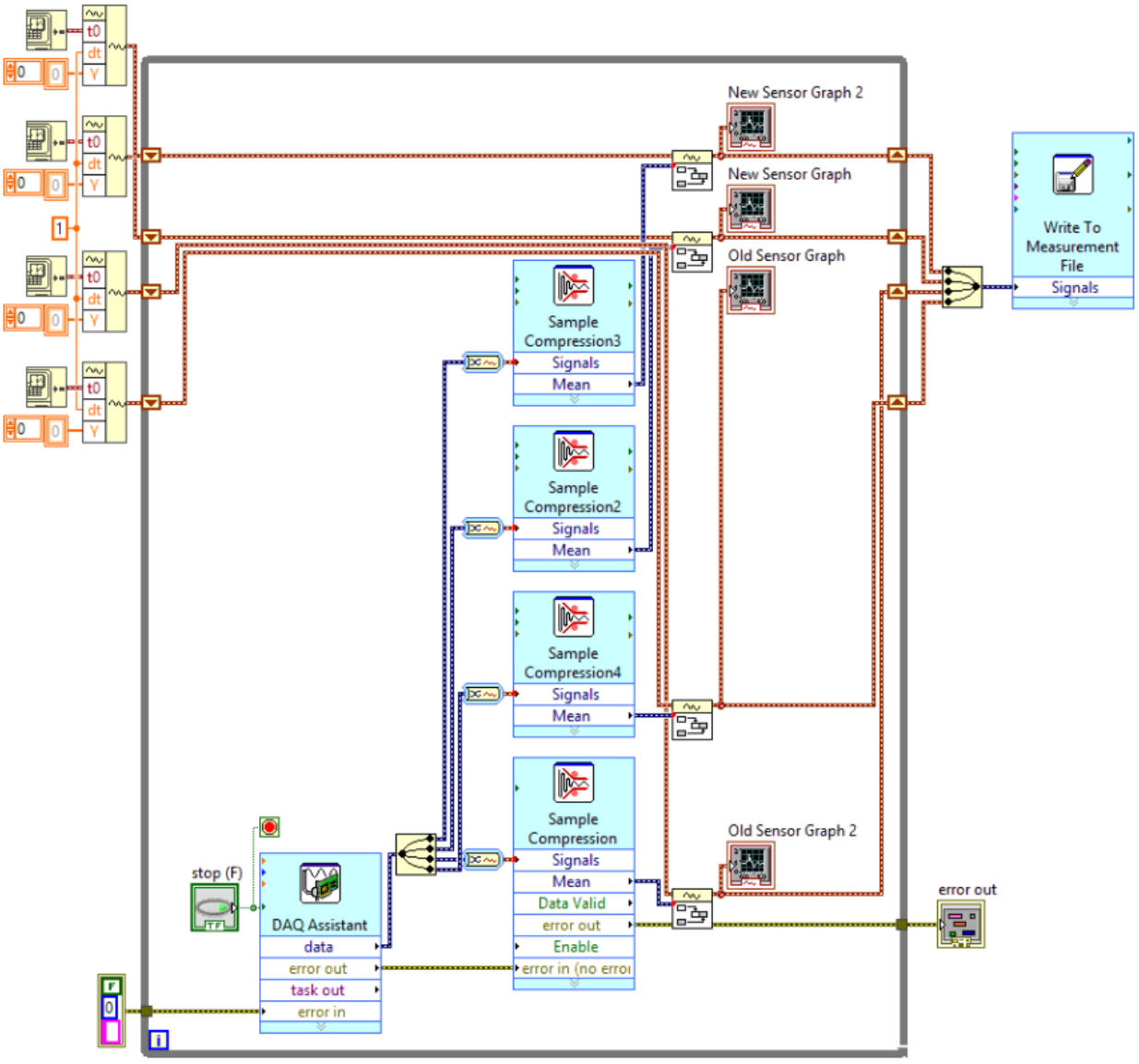

Figure 63 Block diagram of the LabVIEW code used for the pressure data acquisition